

Dynamics of spiral waves in the complex Ginzburg-Landau equation in bounded domains

M. Aguareles

S.J. Chapman

T. Witelski

April 1, 2020

Abstract

Multiple-spiral-wave solutions of the general cubic complex Ginzburg-Landau equation in bounded domains are considered. We investigate the effect of the boundaries on spiral motion under homogeneous Neumann boundary conditions, for small values of the twist parameter q . We derive explicit laws of motion for rectangular domains and we show that the motion of spirals becomes exponentially slow when the twist parameter exceeds a critical value depending on the size of the domain. The oscillation frequency of multiple-spiral patterns is also analytically obtained.

1 Introduction

The complex Ginzburg-Landau equation has a long history in physics. It arises as the amplitude equation in the vicinity of a Hopf bifurcation in spatially-extended systems (see for instance §2 in [13]), and so describes active media close to the onset of pattern formation [4, 12]. The simplest examples of such media are chemical oscillations such as the famous *Belousov-Zhabotinsky* reaction [22]. More complex examples include thermal convection of binary fluids [21], transverse patterns of high intensity light [14]; more recently, it has also been used to model the interaction of several species in some ecological systems [15].

The general cubic complex Ginzburg-Landau equation is given by

$$\frac{\partial \Psi}{\partial t} = \Psi - (1 + ia) |\Psi|^2 \Psi + (1 + ib) \nabla^2 \Psi, \quad (1)$$

where a and b are real parameters and Ψ is a complex field representing the amplitude and phase of the modulations of the oscillatory pattern.

Of particular interest are “defect” solutions of (1) in \mathbb{R}^2 . Solutions with a single defect are characterised by the fact that Ψ has a single zero around which its phase varies by an integer multiple of 2π (that we shall denote as n), known as the winding number. When $a = b$ the isophase lines of such a solution are straight lines emanating from the zero (see [11, 18] for more details). If $a \neq b$, the isophase lines bend to form spirals, left-handed or right-handed depending on the sign of n . The time dependence of this type of solution appears as a global oscillation, so that $\Psi(\mathbf{x}, t) = e^{-i\omega t} \psi(\mathbf{x})$, where ω is not free but needs to be determined as part of the problem. Moreover $\psi(\mathbf{x}) = f(r)e^{in\phi + i\varphi(r)}$, with r and ϕ the polar radial and azimuthal variables respectively, where f and φ satisfy a system of ordinary differential equations (see [11] for the derivation and asymptotic properties of these solutions and [16] for a result on existence and uniqueness of solution).

We are concerned here with solutions containing multiple defects or spirals (we use the terms interchangeably). Such complex patterns may be understood in terms of the position of the

centres of the spirals—if the motion of the defects can be determined, much of the dynamics of the solution can be understood.

Although the time-dependence is now more complicated, it is still convenient to factor out a global phase oscillation from the wavefunction by writing

$$\Psi = e^{-i\omega t} \sqrt{\frac{1+\omega b}{1+ab}} \psi, \quad t = \frac{t'}{1+\omega b}, \quad (x, y) = \sqrt{\frac{1+b^2}{1+b\omega}} (x', y')$$

in (1) to give

$$(1 - ib) \frac{\partial \psi}{\partial t'} = (1 - |\psi|^2) \psi + iq\psi(1 - k^2 - |\psi|^2) + \nabla^2 \psi, \quad (2)$$

where $q = (a - b)/(1 + ab)$ and k is such that

$$q(1 - k^2) = \frac{\omega - b}{1 + b\omega}. \quad (3)$$

The parameters q and k are usually referred to as the *twist parameter* and *asymptotic wavenumber* respectively.

Solutions with finitely-many zeroes evolve in time in such a way that the spirals preserve their local structure (at least for $|n| = 1$, which is the case we consider here). When the twist parameter vanishes (that is if $a = b$), multiple-spiral solutions in \mathbb{R}^2 move on a time-scale that is proportional to the logarithm of the inverse of the typical spiral separation [17]. As q increases (and so $a \neq b$) the interaction weakens and eventually becomes exponentially small in the separation. When q becomes of order one numerical simulations reveal that the dynamics becomes “frozen”, with a set of virtually independent spirals separated by shock lines [6, 7]. The singular role of the twist parameter, as pointed out in [19], is to interpolate between these two very dissimilar behaviours, namely a strong (algebraic) interaction for small values of q and an exponentially weak interaction as q approaches the critical value of $q_c = \pi/(2 \log d)$, where d is the spiral separation, as is shown in [2, 3].

For a finite set of spirals in the whole of \mathbb{R}^2 , the asymptotic wavenumber k represents the wavenumber of the phase of ψ at infinity, that is to say, $k = \lim_{r \rightarrow \infty} \arg(\psi)/r$. Thus expression (3) represents a dispersion relation. Since ω was not free but determined as part of the problem, the same is true of the asymptotic wavenumber k . For small q , on an infinite domain, it turns out that k is exponentially small in q . In our previous work [2, 3] we used perturbation techniques to determine the asymptotic wavenumber and to obtain a law of motion for the centres of an arbitrary arrangement of spirals in the whole of \mathbb{R}^2 .

In this paper we focus on multiple-spiral solutions on a bounded domain in \mathbb{R}^2 when the twist parameter is small. We consider homogeneous Neumann (zero flux) boundary conditions; the extension to periodic boundary conditions is easy to make, and together these cover the vast majority of numerical computations and physical applications. We extend our results in [2, 3] to derive laws of motion for spirals confined to a general bounded domain Ω . The law of motion we find will be given in terms of the Green’s function for a modified Helmholtz equation on Ω , which encodes how the shape of the domain affects the motion of defects. By way of illustration, we then focus on rectangular domains where we obtain explicit laws of motion for a finite set of spirals.

In the limit $q \rightarrow 0$ the interaction of spirals passes from algebraic to exponentially small as separation between spirals increases. To simulate (1) numerically one usually assumes that a large rectangular domain will suffice to approximate the solution on \mathbb{R}^2 . The question then arises as to whether any interesting observed behaviour, such as bound states or a change in the direction or sign of the interaction between spirals, is actually present in \mathbb{R}^2 or is an artifact of truncation.

One of our main results is to show how the size of the domain affects the interaction between spirals. In particular, we find that the motion of spirals becomes exponentially small only when the diameter of the domain approaches $e^{\pi/2q}$, which gives an indication of the difficulty of approximating the solution on an infinite domain with that on a truncated domain.

A second important goal of this paper is to describe the role of the boundaries as a selection mechanism for the oscillation frequency ω , and hence for the asymptotic wavenumber k , which we also obtain. In this case we find that as the diameter of the domain approaches $e^{\pi/2q}$, the asymptotic wavenumber k also shifts from being algebraic to becoming exponentially small in q .

For ease of exposition we shall take $b = 0$ so that, dropping the primes henceforth, the equation we consider is

$$\frac{\partial \psi}{\partial t} = \nabla^2 \psi + (1 - |\psi|^2)\psi + iq\psi(1 - k^2 - |\psi|^2). \quad (4)$$

The paper is organised as follows. Sections 2 and 3 are devoted to obtaining expressions for the laws of motion of the centres of the spirals in general bounded domains. We start in Section 2 by considering what we denote as the *canonical* or *far-field* scale, which corresponds to considering domains of diameter $e^{\pi/2q}$. Then, in Section 3, we consider domains of diameter $\ll e^{\pi/2q}$, which provides a new set of equations for spiral motion in what we denote as the *near field*. In Section 4 we consider the particular case of rectangular domains and we obtain explicit laws of motion in both the far and near field. In particular we find that the interaction between the spirals changes from being exponentially small and mainly in the azimuthal direction when the parameters are in the far field regime to becoming algebraic and with a radial component in the near field. Furthermore, the asymptotic wavenumber of the patterns is exponentially small in the far-field scaling but proportional to the square root of q and the diameter of the domain in the near field. To reconcile these two regimes, a composite law of motion that is valid in both near and far fields is proposed. In Section 5 this composite law of motion is used to compare the trajectories of the spirals with direct numerical simulations of the original system of partial differential equations (4). Finally, in Section 6, we present our conclusions.

2 Interaction of spirals in bounded domains at the canonical scale

In this section we derive laws of motion for the centres of a finite set of spirals with unitary winding numbers confined in general bounded domains with homogeneous Neumann boundary conditions. The law of motion and the corresponding asymptotic wavenumber, k , are given explicitly in terms of the parameter q , which is assumed to be small.

In what follows we assume that the centres of the spirals are separated from each other and from the boundaries by distances which are large in comparison with the core radius of the spirals. By core radius we mean the lengthscale over which the modulus of ψ recovers its equilibrium value close to one (for small q) from its value of zero at the spiral centre. We see from (4) that the core radius is $O(1)$, which means we need the domain to be large if the spirals are to be well-separated. We quantify this by introducing the inverse of the domain diameter as the small parameter ϵ , and we suppose that spirals are separated by distances of $O(1/\epsilon)$.

We therefore consider the system

$$\begin{aligned} \psi_t &= \psi(1 - |\psi|^2) + iq\psi(1 - k^2 - |\psi|^2) + \nabla^2 \psi \quad \text{in } \Omega \\ \frac{\partial \psi}{\partial n} &= 0 \quad \text{on } \partial\Omega, \end{aligned} \quad (5)$$

with parameters $0 < q \ll 1$ and $0 < k \ll 1$. As in unbounded domains (see [2] and [3]), the relationship between ϵ , q and k plays a special role giving place to different types of interaction. In particular, we shall show it is the combination $\alpha = kq/\epsilon$ that determines the nature of the interaction between spirals. In this section we shall assume that α is an order-one constant, and we shall show that this is equivalent to assuming that $1/\epsilon$ is of order $e^{\pi/(2q)}$.

2.1 Outer solution

We follow the same notation as [2] and [3], denoting by $\mathbf{X} = \epsilon \mathbf{x}$ the outer space variable and $T = \mu \epsilon^2 t$ the slow time scale on which the spirals interact. At this stage μ is an unknown small parameter. We will later determine that $\mu = 1/\log(1/\epsilon)$.

Since in this section we are assuming that $\alpha = kq/\epsilon = O(1)$, we write (4) in the outer region as

$$\epsilon^2 \mu \psi_T = (1 + iq) \psi (1 - |\psi|^2) - i \frac{\epsilon^2 \alpha^2}{q} \psi + \epsilon^2 \nabla^2 \psi, \quad \text{in } \Omega$$

along with homogeneous Neumann boundary conditions at the domain boundaries, where ∇ now represents the gradient with respect to \mathbf{X} . We express the solution in amplitude-phase form as $\psi = f e^{i\chi}$, giving

$$\mu \epsilon^2 f_T = \epsilon^2 \nabla^2 f - \epsilon^2 f |\nabla \chi|^2 + f(1 - f^2), \quad (6)$$

$$\mu \epsilon^2 f^2 \chi_T = \epsilon^2 \nabla \cdot (f^2 \nabla \chi) + q f^2 (1 - f^2) - \frac{\epsilon^2 \alpha^2}{q} f^2, \quad (7)$$

in Ω , where now the boundary conditions for f and χ are

$$\frac{\partial f}{\partial n} = \frac{\partial \chi}{\partial n} = 0 \quad \text{on } \partial\Omega.$$

Expanding in power series in ϵ^2 as

$$f(\mathbf{X}, T; \epsilon, q) \sim f_0(\mathbf{X}, T; q) + \epsilon^2 f_1(\mathbf{X}, T; q) + \epsilon^4 f_2(\mathbf{X}, T; q) + \dots,$$

$$\chi(\mathbf{X}, T; \epsilon, q) \sim \chi_0(\mathbf{X}, T; q) + \epsilon^2 \chi_1(\mathbf{X}, T; q) + \epsilon^4 \chi_2(\mathbf{X}, T; q) + \dots,$$

the leading and first-order terms in (6) give

$$f_0 = 1, \quad f_1 = -\frac{1}{2} |\nabla \chi_0|^2. \quad (8)$$

Substituting (8) into (7) gives

$$\begin{aligned} \mu \frac{\partial \chi_0}{\partial T} &= \nabla^2 \chi_0 + q |\nabla \chi_0|^2 - \frac{\alpha^2}{q} \quad \text{in } \Omega \\ \frac{\partial \chi_0}{\partial n} &= 0 \quad \text{on } \partial\Omega. \end{aligned}$$

We proceed as in [3] and expand χ_0 in terms of the small parameter μ as $\chi_0 \sim \frac{1}{q} (\chi_{00} + \mu \chi_{01} + \dots)$ to find, at leading order,

$$\begin{aligned} 0 &= \nabla^2 \chi_{00} + |\nabla \chi_{00}|^2 - \alpha^2 \quad \text{in } \Omega, \\ \frac{\partial \chi_{00}}{\partial n} &= 0 \quad \text{on } \partial\Omega. \end{aligned} \quad (9)$$

Using the Cole-Hopf transformation $\chi_{00} = \log h_0$, equation (9) is transformed into the linear problem

$$\begin{aligned} 0 &= \nabla^2 h_0 - \alpha^2 h_0 \quad \text{in } \Omega, \\ \frac{\partial h_0}{\partial n} &= 0 \quad \text{on } \partial\Omega, \end{aligned} \quad (10)$$

Note that χ_{00} is single-valued (the $n_j\phi$ terms in the phase appear in χ_{01}) so that there is no issue with applying the Cole-Hopf transformation here (unlike in [20]). In order to match to a spiral solution locally near the origin h_0 should have the form $h_0 \sim -\beta \log |\mathbf{X}|$ as $\mathbf{X} \rightarrow \mathbf{0}$ for some constant β [3]. Thus, a solution with N spirals at positions $\mathbf{X}_1, \dots, \mathbf{X}_N$ should satisfy (10) along with

$$h_0 \sim -\beta_j \log |\mathbf{X} - \mathbf{X}_j| \quad \text{as } \mathbf{X} \rightarrow \mathbf{X}_j, \quad \text{for } j = 1, \dots, N. \quad (11)$$

The solution to (10)-(11) is therefore

$$h_0 = -2\pi \sum_{j=1}^N \beta_j G_n(\mathbf{X}; \mathbf{X}_j) = \mathcal{G}(\mathbf{X}; \alpha(T), \beta_1(T), \dots, \beta_N(T), \mathbf{X}_1(T), \mathbf{X}_2(T), \dots, \mathbf{X}_N(T)), \quad (12)$$

say, where $G_n(\mathbf{X}; \mathbf{Y})$ is the Neumann Green's function for the modified Helmholtz equation in Ω , satisfying

$$\nabla^2 G_n - \alpha^2 G_n = \delta(\mathbf{X} - \mathbf{Y}) \quad \text{in } \Omega, \quad \frac{\partial G_n}{\partial n} = 0 \quad \text{on } \partial\Omega, \quad (13)$$

and we have been explicit about the dependence of \mathcal{G} on the value of α , the weights β_j , and the position of the spirals \mathbf{X}_j , all of which may depend on T .

2.2 Inner solution

We rescale close to the centre of a spiral \mathbf{X}_ℓ by writing $\mathbf{X} = \mathbf{X}_\ell + \epsilon \bar{\mathbf{x}}$ to give

$$\begin{aligned} \epsilon \mu \left(\epsilon f_T - \frac{d\mathbf{X}_\ell}{dT} \cdot \nabla f \right) &= \nabla^2 f - f |\nabla \chi|^2 + (1 - f^2)f, \\ \epsilon \mu f^2 \left(\epsilon \chi_T - \frac{d\mathbf{X}_\ell}{dT} \cdot \nabla \chi \right) &= \nabla \cdot (f^2 \nabla \chi) + q(1 - f^2)f^2 - \frac{\epsilon^2 \alpha^2 f^2}{q}, \end{aligned}$$

or equivalently

$$\epsilon \mu \left(\epsilon \psi_T - \frac{d\mathbf{X}_\ell}{dT} \cdot \nabla \psi \right) = \nabla^2 \psi + (1 + iq)(1 - |\psi|^2)\psi - i \frac{\epsilon^2 \alpha^2}{q} \psi,$$

where ∇ represents now the gradient with respect to the inner variable $\bar{\mathbf{x}}$. Since we assume that the distance between the spiral centre and the boundary is much greater than the core radius, the inner equations must be solved on an unbounded domain, with conditions at infinity that come from matching with the outer solution. Thus the solution in the inner region mirrors that in [3].

Expanding $f \sim f_0(\bar{\mathbf{x}}; q, \mu) + \epsilon f_1(\bar{\mathbf{x}}; q, \mu) + \epsilon^2 f_2(\bar{\mathbf{x}}; q, \mu) + \dots$ and $\chi \sim \chi_0(\bar{\mathbf{x}}; q, \mu) + \epsilon \chi_1(\bar{\mathbf{x}}; q, \mu) + \dots$, or equivalently $\psi \sim \psi_0(\bar{\mathbf{x}}; q, \mu) + \epsilon \psi_1(\bar{\mathbf{x}}; q, \mu) + \dots$, the leading-order equation is

$$0 = \nabla^2 \psi_0 + (1 + iq)\psi_0(1 - |\psi_0|^2),$$

with solution $f_0 = f_0(r, T)$ and $\chi_0 = n_\ell \phi + \varphi_0(r, T)$, where r and ϕ are the radial and azimuthal variables with respect to the spiral's centre, $|n_\ell| = 1$ is the spiral's winding number, and f_0

and φ_0 satisfy ordinary differential equations in r which depend on the small parameter q . Expanding further in q as $f_0 \sim f_{00} + f_{01}q + f_{02}q^2 + \dots$ and $\varphi_0 \sim \varphi_{00}/q + \varphi_{01} + \varphi_{02}q + \dots$, gives $\varphi_{00} = \varphi_{00}(T)$, $\varphi_{01} = \varphi_{01}(T)$ and also

$$f_{00}'' + \frac{f_{00}'}{r} - \frac{f_{00}}{r^2} + (1 - f_{00}^2)f_{00} = 0, \quad (14)$$

$$\varphi_{02}'(r) = -\frac{1}{rf_{00}^2} \int_0^r s f_{00}^2 (1 - f_{00}^2) ds, \quad (15)$$

with boundary conditions $f_{00}(0) = 0$ and, to match with (8), $\lim_{r \rightarrow \infty} f_{00}(r) = 1$. Note that we allow the (constant in space) terms φ_{00}/q and φ_{01} in order to enable φ to match with the outer solution $\chi_0 \sim \chi_{00}/q$ (though we fact we will not worry about these terms further since we can obtain all the information we need by matching derivatives of φ). The existence of a unique solution for f_{00} has been shown in [10].

At first order in ϵ we find

$$-\mu \frac{d\mathbf{X}_\ell}{dT} \cdot \nabla \psi_0 = \nabla^2 \psi_1 + (1 + iq)(\psi_1(1 - 2|\psi_0|^2) - \psi_0^2 \psi_1^*), \quad (16)$$

or equivalently, in terms of f_1 and χ_1 ,

$$-\mu \frac{d\mathbf{X}_\ell}{dT} \cdot \nabla f_0 = \nabla^2 f_1 - f_1 |\nabla \chi_0|^2 - 2f_0 \nabla \chi_0 \cdot \nabla \chi_1 + f_1 - 3f_0^2 f_1, \quad (17)$$

$$-\mu f_0^2 \frac{d\mathbf{X}_\ell}{dT} \cdot \nabla \chi_0 = \nabla \cdot (f_0^2 \nabla \chi_1) + \nabla \cdot (2f_0 f_1 \nabla \chi_0) + 2q f_0 f_1 - 4q f_0^3 f_1. \quad (18)$$

Note that we retain the terms proportional to μ in these equations since we will later find that $\mu = O(q) = O(1/|\log \epsilon|)$.

2.3 Inner limit of the outer

We define the regular part of the outer solution \mathcal{G} near the ℓ th spiral by setting

$$\mathcal{G}_{\text{reg}}^\ell(\mathbf{X}) = \mathcal{G}(\mathbf{X}) + \beta_\ell \log |\mathbf{X} - \mathbf{X}_\ell(T)|. \quad (19)$$

Then, from (12), as \mathbf{X} approaches \mathbf{X}_ℓ , we find

$$h_0 \sim -\beta_\ell \log |\mathbf{X} - \mathbf{X}_\ell| + \mathcal{G}_{\text{reg}}^\ell(\mathbf{X}_\ell) + (\mathbf{X} - \mathbf{X}_\ell) \cdot \nabla \mathcal{G}_{\text{reg}}^\ell(\mathbf{X}_\ell) + \dots$$

Thus, written in terms of the inner variables,

$$\chi_0 \sim \frac{1}{q} \log h_0 \sim \frac{1}{q} \log \left(-\beta_\ell \log(\epsilon r) + \mathcal{G}_{\text{reg}}^\ell(\mathbf{X}_\ell) \right) + \frac{\epsilon \bar{\mathbf{x}} \cdot \nabla \mathcal{G}_{\text{reg}}^\ell(\mathbf{X}_\ell)}{q (-\beta_\ell \log(\epsilon r) + \mathcal{G}_{\text{reg}}^\ell(\mathbf{X}_\ell))} + \dots, \quad (20)$$

where $r = R/\epsilon = |\mathbf{X} - \mathbf{X}_\ell(T)|/\epsilon$.

2.4 Outer limit of the inner

Using (15) along with the fact that $f_{00} \sim 1 - 1/r^2$ as $r \rightarrow \infty$, it is found that

$$\frac{\partial \varphi_{02}}{\partial r} \sim -q \frac{\log r + c_1}{r} + \dots, \quad (21)$$

as $r \rightarrow \infty$, where c_1 is a constant given by [11]

$$c_1 = \lim_{r \rightarrow \infty} \left(\int_0^r f_0^2(s) (1 - f_0(s)^2) s ds - \log r \right) \approx -0.098.$$

However, in order to match with the outer expansion we need the outer limit of the whole expansion in q . This can be found to be of the form

$$f_0 \sim 1 + \frac{1}{r^2} \sum_{i=0}^N C_i (q(\log r + c_1))^{2i} + \dots, \quad (22)$$

$$\frac{\partial \chi_0}{\partial r} \sim -\frac{1}{r} \sum_{i=0}^N D_i (q(\log r + c_1))^{2i+1} + \dots, \quad (23)$$

where $C_i > 0$ and $D_i > 0$ are constant values independent of q . The necessity of taking all the terms in q when matching can be seen, since the expansion in q is valid only when $q(\log r + c_1) \ll 1$. When $\alpha = O(1)$, q turns out to be $O(1/\log \epsilon)$ and thus all the terms in (22)–(23) are the same order. We can sum all these terms in the outer limit of the inner expansion using the same method as in Section 3.3.1 in [3]. The idea is to rewrite the leading-order (in ϵ) inner equations in terms of the outer variable $R = \epsilon r$ to obtain

$$0 = \epsilon^2 (\nabla^2 f_0 - f_0 |\nabla \chi_0|^2) + (1 - f_0^2) f_0, \quad (24)$$

$$0 = \epsilon^2 \nabla \cdot (f_0^2 \nabla \chi_0) + q(1 - f_0^2) f_0^2. \quad (25)$$

We now expand again in powers of ϵ as $\chi_0 \sim \hat{\chi}_{00}(r, \phi; q) + \epsilon^2 \hat{\chi}_{01}(r, \phi; q) + \dots$ and $f_0 \sim \hat{f}_{00}(r, \phi; q) + \epsilon^2 \hat{f}_{01}(r, \phi; q) + \dots$. The leading-order term in this expansion $\hat{\chi}_{00}(r, \phi; q)$ is just the first term (in ϵ) in the outer expansion of the leading-order (in ϵ) inner solution, including all the terms in q . Substituting these expansions into (24)–(25) gives $\hat{f}_{00} = 1$, $\hat{f}_{01} = -\frac{1}{2} |\nabla \hat{\chi}_{00}|^2$ and

$$0 = \nabla^2 \hat{\chi}_{00} + q |\nabla \hat{\chi}_{00}|^2,$$

that is a Riccati equation which can be linearised with the change of variable $\hat{\chi}_{00} = (1/q) \log \hat{h}_0$ to give $\nabla^2 \hat{h}_0 = 0$.

Since $\hat{\chi}_{00} = n_\ell \phi + \hat{\varphi}(R)$ we set $\hat{h}_0 = e^{qn_\ell \phi} e^{q\hat{\varphi}(R)} = e^{qn_\ell \phi} H_0(R)$ to give

$$H_0'' + \frac{H_0'}{R} + q^2 \frac{H_0}{R^2} = 0,$$

with solution

$$H_0 = A_\ell(q) \epsilon^{-iqn_\ell} R^{iqn_\ell} + B_\ell(q) \epsilon^{iqn_\ell} R^{-iqn_\ell}, \quad (26)$$

where A_ℓ and B_ℓ are constants that depend on q which may be different at each vortex, and the factors $\epsilon^{\pm iqn_\ell}$ are included to facilitate their determination by comparison with the solution in the inner variable. To determine A_ℓ and B_ℓ we need to write $\hat{\chi}_{00}$ in terms of r , expand in powers of q , and compare with (21). Writing the constants in powers of q as $A_\ell(q) \sim A_{\ell 0}/q + A_{\ell 1} + qA_{\ell 2} + \dots$ and $B_\ell(q) \sim B_{\ell 0}/q + B_{\ell 1} + qB_{\ell 2} + \dots$, and expressing H_0 in terms of r we find

$$\begin{aligned} H_0(r) &= A_\ell(q) e^{iqn_\ell \log r} + B_\ell(q) e^{-iqn_\ell \log r} \\ &\sim \frac{A_{\ell 0} + B_{\ell 0}}{q} + A_{\ell 1} + B_{\ell 1} + (A_{\ell 0} - B_{\ell 0}) i n_\ell \log r \\ &\quad + q \left(A_{\ell 2} + B_{\ell 2} + (A_{\ell 1} - B_{\ell 1}) i n_\ell \log r - \frac{(A_{\ell 0} + B_{\ell 0})}{2} \log^2 r \right) + \dots, \end{aligned}$$

so that

$$\begin{aligned} \frac{\partial \hat{\chi}_{00}}{\partial r} &= \frac{H_0'(r)}{q H_0(r)} \sim \frac{n_\ell (A_{\ell 0} - B_{\ell 0}) i}{r (A_{\ell 0} + B_{\ell 0})} + q \left(\frac{(A_{\ell 1} - B_{\ell 1}) n_\ell i}{(A_{\ell 0} + B_{\ell 0}) r} - \frac{\log r}{r} \right. \\ &\quad \left. + \frac{(A_{\ell 0} - B_{\ell 0})^2 \log r}{(A_{\ell 0} + B_{\ell 0})^2 r} - \left(\frac{i(A_{\ell 0} - B_{\ell 0})(A_{\ell 1} + B_{\ell 1})}{(A_{\ell 0} + B_{\ell 0})^2} \right) \frac{n_\ell}{r} \right) + \dots \end{aligned}$$

Comparing with (21) (and recalling that $n_\ell = \pm 1$) we see that

$$A_{\ell 0} - B_{\ell 0} = 0, \quad (27)$$

$$\frac{(A_{\ell 1} - B_{\ell 1})}{A_{\ell 0} + B_{\ell 0}} \mathbf{i} = -n_\ell c_1 \quad \text{for } \ell = 1, \dots, N. \quad (28)$$

The remaining equations determining A_ℓ and B_ℓ will be fixed when matching with the outer region.

Outer limit of the first-order inner We do the same with the first-order (in ϵ) inner solution. The details of the calculations, which we summarize in what follows, are the same as in Section 4.3.4 in [3]. We first write equation (17)-(18) in terms of the outer variable to give

$$\begin{aligned} -\epsilon \mu \frac{d\mathbf{X}_\ell}{dT} \cdot \nabla f_0 &= \epsilon^2 \nabla^2 f_1 - \epsilon^2 f_1 |\nabla \chi_0|^2 - 2\epsilon^2 f_0 \nabla \chi_0 \cdot \nabla \chi_1 + f_1 - 3f_0^2 f_1, \\ -\mu \epsilon f_0^2 \frac{d\mathbf{X}_\ell}{dT} \cdot \nabla \chi_0 &= \epsilon^2 \nabla \cdot (f_0^2 \nabla \chi_1) + \epsilon^2 \nabla \cdot (2f_0 f_1 \nabla \chi_0) + 2q f_0 f_1 - 4q f_0^3 f_1. \end{aligned}$$

We now expand in powers of ϵ as $\chi_1 \sim \hat{\chi}_{10}(r, \phi; q)/\epsilon + \hat{\chi}_{11}(r, \phi; q) + \dots$ and $f_1 \sim \hat{f}_{10}(r, \phi; q) + \epsilon \hat{f}_{11}(r, \phi; q) + \dots$ to give $\hat{f}_{10} = 0$, $\hat{f}_{11} = -\nabla \hat{\chi}_{00} \cdot \nabla \hat{\chi}_{10}$ and

$$-\mu \frac{d\mathbf{X}_\ell}{dT} \cdot \nabla \hat{\chi}_{00} = \nabla^2 \hat{\chi}_{10} + 2q \nabla \hat{\chi}_{00} \cdot \nabla \hat{\chi}_{10}. \quad (29)$$

Motivated by the transformation we applied to $\hat{\chi}_{00}$ we write $\hat{\chi}_{10} = \hat{h}_1/(q\hat{h}_0) = \hat{h}_1 e^{-q\hat{\chi}_{00}}/q$ and (29) becomes

$$-\mu \frac{d\mathbf{X}_\ell}{dT} \cdot \nabla \hat{\chi}_{00} = \frac{e^{-q\hat{\chi}_{00}}}{q} \nabla^2 \hat{h}_1.$$

Writing $\hat{\chi}_{00}$ in terms of \hat{h}_0 gives

$$-\mu \frac{d\mathbf{X}_\ell}{dT} \cdot \nabla \hat{h}_0 = \nabla^2 \hat{h}_1. \quad (30)$$

Writing the velocity as

$$\frac{d\mathbf{X}_\ell}{dT} = (V_1, V_2)$$

and recalling that $\hat{h}_0 = e^{qn_\ell \phi} H_0(R)$, the left hand side of (30) gives

$$\begin{aligned} -\mu \frac{d\mathbf{X}_\ell}{dT} \cdot \left(\frac{qn_\ell e^{qn_\ell \phi} H_0(R)}{R} \mathbf{e}_\theta + H'_0(R) e^{qn_\ell \phi} \mathbf{e}_R \right) \\ = -\frac{\mu q n_\ell e^{qn_\ell \phi}}{R} \left(e^{i\phi} R^{iqn_\ell} A_\ell \epsilon^{-iqn_\ell} (V_2 + iV_1) - e^{-i\phi} R^{-iqn_\ell} B_\ell \epsilon^{iqn_\ell} (V_2 - iV_1) \right), \end{aligned}$$

since

$$\begin{aligned} \frac{H_0(R)}{R} &= A_\ell(q) \epsilon^{-iqn_\ell} R^{iqn_\ell-1} + B_\ell(q) \epsilon^{iqn_\ell} R^{-iqn_\ell-1}, \\ H'_0(R) &= iqn_\ell A_\ell(q) \epsilon^{-iqn_\ell} R^{iqn_\ell-1} - iqn_\ell B_\ell(q) \epsilon^{iqn_\ell} R^{-iqn_\ell-1}. \end{aligned}$$

Therefore, writing

$$\hat{h}_1 = -\mu q n_\ell A_\ell \epsilon^{-iqn_\ell} (V_2 + iV_1) g_1(R) e^{(qn_\ell + i)\phi} - \mu q n_\ell B_\ell \epsilon^{iqn_\ell} (V_2 - iV_1) g_2(R) e^{(qn_\ell - i)\phi},$$

yields a system of ordinary differential equations for g_1 and g_2 , whose solution gives

$$\begin{aligned}\widehat{h}_1 = & -\frac{\mu A_\ell \epsilon^{-iqn_\ell}(V_1 - iV_2)}{4}(R^{iqn_\ell+1} + \gamma_1 R^{1-iqn_\ell})e^{(qn_\ell+i)\phi} \\ & -\frac{\mu B_\ell \epsilon^{iqn_\ell}(V_1 + iV_2)}{4}(R^{-iqn_\ell+1} + \gamma_2 R^{1+iqn_\ell})e^{(qn_\ell-i)\phi}.\end{aligned}\quad (31)$$

where γ_1 and γ_2 are unknown constants that will be determined by matching to the inner limit of the outer solution.

2.5 Leading order matching: determination of the asymptotic wavenumber

Using (26) and (27), the leading-order (in ϵ) outer limit of the inner expansion is found to be,

$$\widehat{\chi}_{00} \sim \frac{1}{q} \log H_0 + O(1) \sim \frac{1}{q} \log \left(\frac{A_{0\ell} e^{-iqn_\ell \log \epsilon} + A_{0\ell} e^{iqn_\ell \log \epsilon}}{q} + O(1) \right),$$

while the leading-order inner limit of the outer, according to (20) reads

$$\chi_{00} \sim \frac{1}{q} \log \left(-\beta_\ell \log(\epsilon r) + \mathcal{G}_{\text{reg}}^\ell(\mathbf{X}_\ell) + O(\epsilon r) \right). \quad (32)$$

Hence, in order to match, the order $1/q$ term inside the logarithm in the outer limit of the inner must vanish, so that

$$e^{-iqn_\ell \log \epsilon} + e^{iqn_\ell \log \epsilon} = O(q) \quad \text{or equivalently} \quad q |\log \epsilon| = \frac{\pi}{2} + q\nu, \quad (33)$$

where ν is an order one constant and $|n_\ell| = 1$. This expression provides a relation between the two small parameters q and ϵ , and it is needed in order for α to be an order one constant. It is equivalent to assuming that the typical size domain is $1/\epsilon = O(e^{\pi/2q})$.

The outer limit of the inner now reads

$$\widehat{\chi}_{00} \sim \frac{1}{q} \log (-2A_{0\ell}\nu + in_\ell(A_{1\ell} - B_{1\ell}) - 2A_{0\ell} \log R + \dots),$$

and matching with (32) provides the conditions $A_{0\ell} = \beta_\ell/2$ and

$$\mathcal{G}_{\text{reg}}^\ell(\mathbf{X}_\ell) = -2A_{0\ell}\nu + in_\ell(A_{1\ell} - B_{1\ell}).$$

Eliminating $A_{1\ell} - B_{1\ell}$ using (28) gives

$$\mathcal{G}_{\text{reg}}^\ell(\mathbf{X}_\ell) + \beta_\ell(c_1 + \nu) = 0. \quad (34)$$

With ν given by (33), and for a given set of spiral positions \mathbf{X}_ℓ , equation (34) provides a set of N equations for the $N + 1$ unknowns α and β_ℓ , $\ell = 1, \dots, N$ (recall that $\mathcal{G}_{\text{reg}}^\ell(\mathbf{X}_\ell)$, defined through (12), (13) and (19), depends on α and β_1, \dots, β_N). However, since $\mathcal{G}_{\text{reg}}^\ell(\mathbf{X}_\ell)$ is a homogeneous, linear function of β_1, \dots, β_N (see (12)), the system (34) is a homogeneous linear system of N equations for β_1, \dots, β_N . There exists a solution if and only if the determinant of the system is zero, which provides an equation for α . This in turn determines the asymptotic wavenumber, $k = \alpha\epsilon/q$, and therefore the oscillation frequency ω . The coefficients β_1, \dots, β_N are then determined only up to some global scaling (which is equivalent to adding a constant to χ_{00}).

2.6 First order matching: law of motion for the centres of the spirals

We now compare one term of the outer ϵ -expansion with two terms of the inner ϵ -expansion (in the notation of Van Dyke [9]). This matching will eventually provide a law of motion for the spirals.

The two-term inner expansion of the one-term outer solution for χ is given in (20). We must compare this with the one-term outer expansion of the two-term inner solution $\chi_0 + \epsilon\chi_1$. From §2.4 the one-term (in ϵ) outer expansion of this is

$$\frac{1}{q} \log(\widehat{h}_0) + \frac{\widehat{h}_1}{q\widehat{h}_0}. \quad (35)$$

Comparing this with (20) gives the matching condition

$$\bar{\mathbf{x}} \cdot \nabla \mathcal{G}_{\text{reg}}^\ell(\mathbf{X}_\ell) = \frac{\mu r i n_\ell A_{0\ell}}{4q} \left(e^{i\phi}(V_1 - iV_2)(1 + \gamma_1) - e^{-i\phi}(V_1 + iV_2)(1 + \gamma_2) \right).$$

Note that this equation implies that $\mu = O(q)$, as we have been supposing. Solving for γ_1 and γ_2 , substituting into (31), writing $\widehat{\chi}_{10}$ in terms of the inner variable and expanding in powers of q finally gives, to leading order in q ,

$$\chi_{10} \sim -\frac{\mu r}{2q}(V_1 \cos \phi + V_2 \sin \phi) + \frac{n_\ell r}{\beta_\ell} \nabla \mathcal{G}_{\text{reg}}^\ell(\mathbf{X}_\ell) \cdot \mathbf{e}_\phi \quad \text{as } r \rightarrow \infty. \quad (36)$$

Solvability condition and law of motion Equation (36) provides a boundary condition on the first-order inner equation (16). However, there is a solvability condition on (16) subject to (36), which determines V_1 and V_2 , thereby providing our law of motion for the spiral centres. The analysis in this section summarises the corresponding analysis in [3].

Multiplying equation (16) by the conjugate v^* of a solution v of the adjoint equation

$$\nabla^2 v + (1 - iq)(v(1 - 2|\psi_0|^2) - \psi_0^2 v^*) = 0,$$

integrating over a disk B_{r^*} of radius r^* , and using integration by parts gives, after some manipulation,

$$-\int_{B_{r^*}} \Re \left\{ (1 - iq) \mu v^* \frac{d\mathbf{X}_\ell}{dT} \cdot \nabla \psi_0 \right\} dS = \int_{\partial B_{r^*}} \Re \left\{ (1 - iq) \left(v^* \frac{\partial \psi_1}{\partial n} - \frac{\partial v^*}{\partial n} \psi_1 \right) \right\} ds, \quad (37)$$

where \Re denotes the real part. A straightforward calculation shows that directional derivatives of ψ_0 are solutions of the adjoint problem if q is replaced by $-q$, i.e. $v = \mathbf{d} \cdot \nabla \psi_0|_{q \rightarrow -q}$, where \mathbf{d} is any vector in \mathbb{R}^2 . To leading order in q and μ the solvability condition (37) is

$$0 = \int_{\partial B_{r^*}} \Re \left\{ (\mathbf{d} \cdot \nabla \psi_0^*) \frac{\partial \psi_1}{\partial n} - \frac{\partial (\mathbf{d} \cdot \nabla \psi_0^*)}{\partial n} \psi_1 \right\} ds.$$

Letting the disk radius r^* tend to infinity gives

$$\lim_{r \rightarrow \infty} \int_0^{2\pi} (\mathbf{e}_\phi \cdot \mathbf{d}) \left(\frac{\partial \chi_{10}}{\partial r} + \frac{\chi_{10}}{r} \right) d\phi = 0. \quad (38)$$

Now using (36) gives the law of motion, to leading order in q ,

$$\frac{d\mathbf{X}_\ell}{dT} = -\frac{2qn_\ell}{\beta_\ell \mu} \nabla^\perp \mathcal{G}_{\text{reg}}^\ell(\mathbf{X}_\ell), \quad (39)$$

where $\nabla^\perp = (-\partial_y, \partial_x)$.

Summary The parameter α and the coefficients β_j are determined (up to a scaling) by the linear system (34), which is

$$2\pi\beta_\ell G_{\text{n,reg}}(\mathbf{X}_\ell; \mathbf{X}_\ell) + 2\pi \sum_{j=1, j \neq \ell}^N \beta_j G_{\text{n}}(\mathbf{X}_\ell; \mathbf{X}_j) - \beta_\ell(c_1 + \nu) = 0, \quad (40)$$

where

$$G_{\text{n,reg}}(\mathbf{X}; \mathbf{Y}) = G_{\text{n}}(\mathbf{X}; \mathbf{Y}) - \frac{1}{2\pi} \log |\mathbf{X} - \mathbf{Y}|,$$

is the regular part of the Neumann Green's function G_{n} for the modified Helmholtz equation

$$\nabla^2 G_{\text{n}} - \alpha^2 G_{\text{n}} = \delta(\mathbf{X} - \mathbf{Y}) \quad \text{in } \Omega, \quad \frac{\partial G_{\text{n}}}{\partial n} = 0 \quad \text{on } \partial\Omega, \quad (41)$$

and $\nu = \log(1/\epsilon) - \pi/2q$. The law of motion (39) may be written, to leading order in q , as

$$\frac{d\mathbf{X}_\ell}{dT} = \frac{4\pi q n_\ell}{\beta_\ell \mu} \sum_{j=1, j \neq \ell}^N \beta_j \nabla^\perp G_{\text{n}}(\mathbf{X}_\ell; \mathbf{X}_j) + \frac{4\pi q n_\ell}{\mu} \nabla^\perp G_{\text{n,reg}}(\mathbf{X}_\ell; \mathbf{X}_\ell) \quad (42)$$

As the size of the domain tends to infinity,

$$G_{\text{n}}(\mathbf{X}; \mathbf{Y}) \sim -\frac{1}{2\pi} K_0(\alpha |\mathbf{X} - \mathbf{Y}|), \quad (43)$$

where K_0 is the order zero modified Bessel function of second kind, and equation (42) agrees with that given in [2] for spirals in an infinite domain.

3 Interaction of spirals in bounded domains in the near-field

In the previous section we assumed the parameter α is order one as $\epsilon \rightarrow 0$, which led to q and ϵ being related by (33), which implies that the separation of spirals, and therefore the size of the domain, is exponentially large in q .

We now consider smaller domains, in which α will be small. In the limit $q, \epsilon \rightarrow 0$ with $0 < q \log(1/\epsilon) < \pi/2$ we will find that $\alpha = O(q^{1/2})$. This is in contrast to spirals in the near field in the whole of \mathbb{R}^2 , where α is found to be exponentially small in q [2].

3.1 Outer region

As before we rescale time as $T = \mu\epsilon^2 t$ and use $\mathbf{X} = \epsilon\mathbf{x}$ as the outer variable, to give

$$\epsilon^2 \mu \psi_T = (1 + iq) \psi(1 - |\psi|^2) - i \frac{\epsilon^2 \alpha^2}{q} \psi + \epsilon^2 \nabla^2 \psi \quad \text{in } \Omega.$$

Recall that $1/\epsilon$ is the typical domain diameter in \mathbf{x} , so that the diameter of the domain is $O(1)$ in terms of \mathbf{X} . Expressing the solution in amplitude-phase form as $\psi = f e^{i\chi}$ yields

$$\mu \epsilon^2 f_T = \epsilon^2 \nabla^2 f - \epsilon^2 f |\nabla \chi|^2 + f(1 - f^2), \quad (44)$$

$$\mu \epsilon^2 f^2 \chi_T = \epsilon^2 \nabla \cdot (f^2 \nabla \chi) + q f^2 (1 - f^2) - \frac{\epsilon^2 \alpha^2}{q} f^2, \quad (45)$$

in Ω , where, as before, the boundary conditions for f and χ are

$$\frac{\partial f}{\partial n} = \frac{\partial \chi}{\partial n} = 0 \quad \text{on } \partial\Omega.$$

Expanding in asymptotic power series in ϵ as $f \sim f_0 + \epsilon^2 f_1 + \dots$ and $\chi \sim \chi_0 + \epsilon^2 \chi_1 + \dots$, the leading- and first-order terms in f give

$$f_0 = 1, \quad f_1 = -\frac{1}{2}|\nabla\chi_0|^2.$$

The equation for the leading-order phase function, χ_0 , is

$$\begin{aligned} \mu \frac{\partial \chi_0}{\partial T} &= \nabla^2 \chi_0 + q|\nabla\chi_0|^2 - \frac{\alpha^2}{q} \quad \text{in } \Omega, \\ \frac{\partial \chi_0}{\partial n} &= 0 \quad \text{on } \partial\Omega. \end{aligned}$$

So far the analysis is exactly the same as before. However, we know that α cannot be $O(1)$ this time, and so must be some lower order in q . The natural assumption is that $\alpha^2 = O(q)$, which we will verify a posteriori. We thus rescale $\alpha = q^{1/2}\bar{\alpha}$. We note that α being of order $q^{1/2}$ is consistent with the value of α that is found in [1] for a single spiral in a finite disk with homogeneous Neumann boundary conditions.

Expanding χ_0 in terms of q as $\chi_0 \sim \frac{1}{q}(\chi_{00} + q\chi_{01} + \dots)$ as in §2¹ gives, at leading and first order in q ,

$$0 = \nabla^2 \chi_{00} + |\nabla\chi_{00}|^2, \quad (46)$$

$$\tilde{\mu} \frac{\partial \chi_{00}}{\partial T} = \nabla^2 \chi_{01} + 2\nabla\chi_{00} \cdot \nabla\chi_{01} - \bar{\alpha}^2, \quad (47)$$

in Ω , with homogeneous Neumann boundary conditions, where $\tilde{\mu} = \mu/q$. Integrating (46) over Ω and using the divergence theorem and the boundary conditions gives

$$\int_{\Omega} |\nabla\chi_{00}|^2 dS = 0,$$

so that in fact $\chi_{00} = C_1(T)$. Now (44)-(45) are invariant with respect to the transformation

$$\chi \rightarrow \chi - C_1(T)/q, \quad \alpha^2 \rightarrow \alpha^2 + \mu C_1'(T),$$

so that we may take $C_1 \equiv 0$ without loss of generality. In fact, if $C_1'(T) \neq 0$ it means we have not factored out all the global oscillation when making the change of variables which leads to (2). However, we must be careful when matching with the inner region near each spiral, since changing C_1 is equivalent to scaling A_ℓ in the inner region. With $C_1 = 0$ we will find that the inner expansions for A_ℓ and B_ℓ start at $O(1)$ rather than $O(1/q)$ as they did in §2.4.

The first-order equation (47) becomes

$$\begin{aligned} \nabla^2 \chi_{01} &= \bar{\alpha}^2, \quad \text{in } \Omega, \\ \frac{\partial \chi_{01}}{\partial n} &= 0 \quad \text{on } \partial\Omega, \\ \chi_{01} &\sim C_{2j}(T) \log R_j + n_j \phi_j, \quad \text{as } R_j \rightarrow 0, \quad \text{for } j = 1, \dots, N, \end{aligned} \quad (48)$$

where $R_j = |\mathbf{X} - \mathbf{X}_j(T)|$ and ϕ_j are polar coordinates centred on the j th spiral, and we have assumed that the singularities due to the spirals are locally of the same form as the corresponding singularities when $\Omega = \mathbb{R}^2$ [2]. We thus have a set of unknown slow-time-dependent parameters, $C_{2j}(T)$, one for each spiral, which are determined by matching at each spiral core.

¹Note that in §2 we expanded in μ rather than q . The two expansions are equivalent since $\mu = O(q)$, but it is more natural given we will find $\nabla\chi_{00} = 0$ to expand in q in the present case.

To determine $\bar{\alpha}$ we integrate equation (48) over the domain $V_\delta = \Omega \setminus \sum_{j=1}^N B_\delta(\mathbf{X}_j(T))$, which is the domain that is left after removing disks of radius δ centred at each spiral. Applying the Divergence Theorem on this domain (on which solutions are regular), and then taking the limit $\delta \rightarrow 0$, gives

$$\bar{\alpha}^2 |\bar{\Omega}| = \lim_{\delta \rightarrow 0} \int_{\partial V_\delta} \frac{\partial \chi_{01}}{\partial n} ds = \int_{\partial \Omega} \frac{\partial \chi_{01}}{\partial n} ds + \sum_{j=1}^N \lim_{\delta \rightarrow 0} \int_{\partial B_\delta(\mathbf{X}_j(T))} \frac{\partial \chi_{01}}{\partial n} ds = -2\pi \sum_{j=1}^N C_{2j}, \quad (49)$$

where

$$|\bar{\Omega}| = \int_{\Omega} d\mathbf{X} = \epsilon^2 \int_{\Omega} d\mathbf{x} = \epsilon^2 |\Omega|,$$

is the area of the domain in terms of the outer variable \mathbf{X} .

3.2 Inner region

The inner region is exactly the same as in §2.2.

3.3 Inner limit of the outer

The solution to (48) may be written as

$$\chi_{01} = 2\pi \sum_{j=1}^N C_{2j}(T) \bar{G}_n(\mathbf{X}; \mathbf{X}_j) + 2\pi \sum_{j=1}^N n_j \bar{H}(\mathbf{X}; \mathbf{X}_j) = \bar{\mathcal{G}},$$

say, where $\bar{G}_n(\mathbf{X}; \mathbf{Y})$ is the Neumann Green's function for Laplace's equation in Ω , satisfying

$$\nabla^2 \bar{G}_n = \delta(\mathbf{X} - \mathbf{Y}) - \frac{1}{|\Omega|} \quad \text{in } \Omega, \quad \frac{\partial \bar{G}_n}{\partial n} = 0 \quad \text{on } \partial\Omega, \quad (50)$$

and \bar{H} satisfies

$$\nabla^2 \bar{H} = 0 \quad \text{in } \Omega \setminus \{\mathbf{Y}\}, \quad \frac{\partial \bar{H}}{\partial n} = 0 \quad \text{on } \partial\Omega, \quad \bar{H} \sim \frac{\phi}{2\pi} \text{ as } \mathbf{X} \rightarrow \mathbf{Y},$$

where ϕ is the azimuthal angle centred at \mathbf{Y} . If $\bar{G}_d(\mathbf{X}; \mathbf{Y})$ is the Dirichlet Green's function, satisfying

$$\nabla^2 \bar{G}_d = \delta(\mathbf{X} - \mathbf{Y}) \quad \text{in } \Omega, \quad \bar{G}_d = 0 \quad \text{on } \partial\Omega,$$

then \bar{H} is its harmonic conjugate, so that, with $\mathbf{X} = (X, Y)$,

$$\frac{\partial \bar{H}}{\partial X} = -\frac{\partial \bar{G}_d}{\partial Y}, \quad \frac{\partial \bar{H}}{\partial Y} = \frac{\partial \bar{G}_d}{\partial X}.$$

Defining the regular part of \bar{G}_n , \bar{H} and \bar{G}_d as

$$\begin{aligned} \bar{G}_n(\mathbf{X}; \mathbf{Y}) &= \frac{1}{2\pi} \log |\mathbf{X} - \mathbf{Y}| + \bar{G}_{n,\text{reg}}(\mathbf{X}; \mathbf{Y}), \\ \bar{H}(\mathbf{X}; \mathbf{Y}) &= \frac{\phi}{2\pi} + \bar{H}_{\text{reg}}(\mathbf{X}; \mathbf{Y}), \\ \bar{G}_d(\mathbf{X}; \mathbf{Y}) &= \frac{1}{2\pi} \log |\mathbf{X} - \mathbf{Y}| + \bar{G}_{d,\text{reg}}(\mathbf{X}; \mathbf{Y}), \end{aligned}$$

and

$$\begin{aligned}\overline{\mathcal{G}}_{\text{reg}}^\ell &= 2\pi C_{2\ell}(T)\overline{G}_{\text{n,reg}}(\mathbf{X}; \mathbf{X}_\ell) + 2\pi n_\ell \overline{H}_{\text{reg}}(\mathbf{X}; \mathbf{X}_\ell) \\ &\quad + 2\pi \sum_{j=1, j \neq \ell}^N C_{2j}(T)\overline{G}_{\text{n}}(\mathbf{X}; \mathbf{X}_j) + 2\pi \sum_{j=1, j \neq \ell}^N n_j \overline{H}(\mathbf{X}; \mathbf{X}_j),\end{aligned}\quad (51)$$

we find that as $\mathbf{X} \rightarrow \mathbf{X}_\ell(T)$,

$$\chi_0 \sim n_\ell \phi_\ell + C_{2\ell} \log |\mathbf{X} - \mathbf{X}_\ell(T)| + \overline{\mathcal{G}}_{\text{reg}}^\ell(\mathbf{X}_\ell) + (\mathbf{X} - \mathbf{X}_\ell(T)) \cdot \nabla \overline{\mathcal{G}}_{\text{reg}}^\ell(\mathbf{X}_\ell) + \dots \quad (52)$$

Written in terms of the inner variable $\epsilon \bar{\mathbf{x}} = \mathbf{X} - \mathbf{X}_\ell(T)$ this is

$$\chi_0 \sim n_\ell \phi + C_{2\ell} \log(\epsilon r) + \overline{\mathcal{G}}_{\text{reg}}^\ell(\mathbf{X}_\ell) + \epsilon \bar{\mathbf{x}} \cdot \nabla \overline{\mathcal{G}}_{\text{reg}}^\ell(\mathbf{X}_\ell) + \dots, \quad (53)$$

where r and ϕ are the polar representation of $\bar{\mathbf{x}}$.

3.4 Outer limit of the inner

We sum the q -expansion of the outer limit of the inner in exactly the same way as in §2.4 to give $\hat{\chi}_{00} = n_\ell \phi + (1/q) \log H_0$ with

$$H_0 = A_\ell(q) \epsilon^{-iqn_\ell} R^{iqn_\ell} + B_\ell(q) \epsilon^{iqn_\ell} R^{-iqn_\ell}.$$

To determine A_ℓ and B_ℓ we need to write $\hat{\chi}_{00}$ in terms of r , expand in powers of q , and compare with (21). Crucially though, as mentioned in §3.1, and in contrast to §2.4, the expansions for A_ℓ and B_ℓ proceed now as $A_\ell(q) \sim A_{\ell 0} + qA_{\ell 1} + \dots$ and $B_\ell(q) \sim B_{\ell 0} + qB_{\ell 1} + \dots$. Expressing H_0 in terms of r we find

$$\begin{aligned}H_0(r) &\sim A_{\ell 0} + B_{\ell 0} + q(A_{\ell 1} + B_{\ell 1}) + q(A_{\ell 0} - B_{\ell 0})in_\ell \log r \\ &\quad + q^2 \left(A_{\ell 2} + B_{\ell 2} + (A_{\ell 1} - B_{\ell 1})in_k \log r - \frac{(A_{\ell 0} + B_{\ell 0})}{2} \log^2 r \right) + \dots,\end{aligned}\quad (54)$$

so that

$$\begin{aligned}\frac{\partial \hat{\chi}_{00}}{\partial r} = \frac{H'_0(r)}{qH_0(r)} &\sim \frac{n_\ell(A_{\ell 0} - B_{\ell 0})i}{r(A_{\ell 0} + B_{\ell 0})} + q \left(\frac{(A_{\ell 1} - B_{\ell 1})n_\ell i}{(A_{\ell 0} + B_{\ell 0})r} - \frac{\log r}{r} \right. \\ &\quad \left. + \frac{(A_{\ell 0} - B_{\ell 0})^2 \log r}{(A_{\ell 0} + B_{\ell 0})^2 r} - \frac{i(A_{\ell 0} - B_{\ell 0})(A_{\ell 1} + B_{\ell 1})n_\ell}{(A_{\ell 0} + B_{\ell 0})^2 r} \right) + \dots\end{aligned}$$

Comparing with (21) (and recalling that $n_\ell = \pm 1$) we see that

$$A_{\ell 0} - B_{\ell 0} = 0, \quad (55)$$

$$\frac{(A_{\ell 1} - B_{\ell 1})i}{A_{\ell 0} + B_{\ell 0}} = -n_\ell c_1 \quad \text{for } \ell = 1, \dots, N. \quad (56)$$

The remaining equations determining A_ℓ and B_ℓ will be fixed when matching with the outer region.

Using (55) we now find that (54) gives the outer limit of the leading-order inner expansion as

$$\begin{aligned}\hat{\chi}_{00} &\sim \frac{1}{q} \log \left(A_{0\ell} (e^{-iqn_\ell \log \epsilon} + e^{iqn_\ell \log \epsilon}) \right) + n_\ell \phi + \frac{A_{1\ell} e^{-iqn_\ell \log \epsilon} + B_{1\ell} e^{iqn_\ell \log \epsilon}}{A_{0\ell} (e^{-iqn_\ell \log \epsilon} + e^{iqn_\ell \log \epsilon})} \\ &\quad + in \frac{(e^{-iqn_\ell \log \epsilon} - e^{iqn_\ell \log \epsilon})}{(e^{-iqn_\ell \log \epsilon} + e^{iqn_\ell \log \epsilon})} \log R + O(q).\end{aligned}\quad (57)$$

Similarly, the leading-order outer limit of the first correction to the inner expansion $\hat{\chi}_{10}$ is, as before,

$$\hat{\chi}_{10} \sim -\frac{\mu}{4q}\epsilon r \left(\frac{e^{-iqn_\ell \log \epsilon}(V_1 - iV_2)(1 + \gamma_1)e^{i\phi}}{e^{-iqn_\ell \log \epsilon} + e^{iqn_\ell \log \epsilon}} + \frac{e^{iqn_\ell \log \epsilon}(V_1 + iV_2)(1 + \gamma_2)e^{-i\phi}}{e^{-iqn_\ell \log \epsilon} + e^{iqn_\ell \log \epsilon}} \right).$$

3.5 Leading order matching: determination of the asymptotic wavenumber

Matching (53) with (57) gives

$$0 = \log \left(A_{0\ell}(e^{-iqn_\ell \log \epsilon} + e^{iqn_\ell \log \epsilon}) \right), \quad (58)$$

$$C_{2\ell} = \ln_\ell \frac{(e^{-iqn_\ell \log \epsilon} - e^{iqn_\ell \log \epsilon})}{(e^{-iqn_\ell \log \epsilon} + e^{iqn_\ell \log \epsilon})} = n_\ell \tan(qn_\ell \log \epsilon), \quad (59)$$

$$\bar{\mathcal{G}}_{\text{reg}}(\mathbf{X}_\ell) = \frac{A_{1\ell}e^{-iqn_\ell \log \epsilon} + B_{1\ell}e^{iqn_\ell \log \epsilon}}{A_{0\ell}(e^{-iqn_\ell \log \epsilon} + e^{iqn_\ell \log \epsilon})}. \quad (60)$$

Equation (58) gives $2A_{0\ell} = \text{cosec}(qn_\ell \log \epsilon)$. When $|n_j| = 1$ equation (59) implies the constants C_{2j} are all equal and given by

$$C_{2j} = -\tan(q \log(1/\epsilon)) \quad \forall j.$$

Equations (49) and (59) together determine $\bar{\alpha}$ via

$$\bar{\alpha}^2 = \frac{2\pi}{|\bar{\Omega}|} \sum_{j=1}^N n_j \tan(qn_j \log(1/\epsilon)) = \frac{2\pi N}{|\bar{\Omega}|} \tan(q \log(1/\epsilon)). \quad (61)$$

The asymptotic wavenumber is related to α by $k = \alpha\epsilon/q$ and so, since $\alpha = q^{1/2}\bar{\alpha}$,

$$k = \frac{\epsilon\bar{\alpha}}{q^{1/2}} = \frac{\epsilon}{q^{1/2}} \left(\frac{2\pi N}{|\bar{\Omega}|} \tan(q \log(1/\epsilon)) \right)^{1/2} = \left(\frac{2\pi N}{q|\bar{\Omega}|} \tan(q \log(1/\epsilon)) \right)^{1/2}. \quad (62)$$

As $q \log(1/\epsilon) \rightarrow \pi/2$ this expression matches smoothly into that given by (34); we demonstrate this in Section 4.3 when we develop a uniform composite approximation.

3.6 First order matching: law of motion for the spirals

Matching (53) with (35) gives

$$\begin{aligned} \bar{\mathbf{x}} \cdot \nabla \bar{\mathcal{G}}_{\text{reg}}^\ell(\mathbf{X}_\ell) &\sim \left(\frac{4\gamma_1 - \tilde{\mu}A_{\ell 0}e^{-iqn_\ell \log \epsilon}(V_{1\ell} - iV_{2\ell})}{4(A_{\ell 0}e^{-iqn_\ell \log \epsilon} + B_{\ell 0}e^{iqn_\ell \log \epsilon})} \right) r e^{i\phi} \\ &\quad + \left(\frac{4\gamma_2 - \tilde{\mu}B_{\ell 0}e^{iqn_\ell \log \epsilon}(V_{1\ell} + iV_{2\ell})}{4(A_{\ell 0}e^{-iqn_\ell \log \epsilon} + B_{\ell 0}e^{iqn_\ell \log \epsilon})} \right) r e^{-i\phi}. \end{aligned}$$

Solving for γ_1 and γ_2 and substituting into (35) using (31) gives, finally,

$$\begin{aligned} \chi_{10} &\sim -\frac{\tilde{\mu}r}{4}(V_{1\ell} \cos \phi + V_{2\ell} \sin \phi) + \frac{\tilde{\mu}r}{4}(V_{1\ell} \cos(\phi - 2qn_\ell \log \epsilon) + V_{2\ell} \sin(\phi - 2qn_\ell \log \epsilon)) \\ &\quad + r \cos(qn_\ell \log \epsilon) \left(\frac{\partial \bar{\mathcal{G}}_{\text{reg}}^\ell}{\partial X}(\mathbf{X}_\ell) \cos(\phi - qn_\ell \log \epsilon) + \frac{\partial \bar{\mathcal{G}}_{\text{reg}}^\ell}{\partial Y}(\mathbf{X}_\ell) \sin(\phi - qn_\ell \log \epsilon) \right) \end{aligned} \quad (63)$$

The compatibility condition (38) then gives the law of motion as

$$\frac{d\mathbf{X}_\ell}{dT} = \frac{2}{\tilde{\mu}} \cot(qn_\ell \log \epsilon) \nabla^\perp \overline{\mathcal{G}}_\text{reg}^\ell(\mathbf{X}_\ell). \quad (64)$$

Using (51) and (59) we may write this as

$$\begin{aligned} \frac{\tilde{\mu}}{2} \tan(qn_\ell \log \epsilon) \frac{d\mathbf{X}_\ell}{dT} &= 2\pi(n_\ell \tan(qn_\ell \log \epsilon)) \nabla^\perp \overline{\mathcal{G}}_{\text{n,reg}}(\mathbf{X}_\ell; \mathbf{X}_\ell) + 2\pi n_\ell \nabla^\perp \overline{H}_\text{reg}(\mathbf{X}_\ell; \mathbf{X}_\ell) \\ &\quad + 2\pi \sum_{j=1, j \neq \ell}^N (n_j \tan(qn_j \log \epsilon)) \nabla^\perp \overline{\mathcal{G}}_\text{n}(\mathbf{X}_\ell; \mathbf{X}_j) \\ &\quad + 2\pi \sum_{j=1, j \neq \ell}^N n_j \nabla^\perp \overline{H}(\mathbf{X}_\ell; \mathbf{X}_j) \\ &= 2\pi n_\ell \tan(qn_\ell \log \epsilon) \nabla^\perp \overline{\mathcal{G}}_{\text{n,reg}}(\mathbf{X}_\ell; \mathbf{X}_\ell) - 2\pi n_\ell \nabla \overline{\mathcal{G}}_{\text{d,reg}}(\mathbf{X}_\ell; \mathbf{X}_\ell) \\ &\quad + 2\pi \sum_{j=1, j \neq \ell}^N n_j \tan(qn_j \log \epsilon) \nabla^\perp \overline{\mathcal{G}}_\text{n}(\mathbf{X}_\ell; \mathbf{X}_j) \\ &\quad - 2\pi \sum_{j=1, j \neq \ell}^N n_j \nabla \overline{\mathcal{G}}_\text{d}(\mathbf{X}_\ell; \mathbf{X}_j). \end{aligned} \quad (65)$$

Thus we see the motion due to each spiral is a mix of the gradient of the Dirichlet Green's function and the perpendicular gradient of the Neumann Green's function.

Since we are considering only the case that $|n_j| = 1$ for all j we may simplify to

$$\begin{aligned} n_\ell \frac{\mu}{2q} \tan(q \log \epsilon) \frac{d\mathbf{X}_\ell}{dT} &= 2\pi \tan(q \log \epsilon) \nabla^\perp \overline{\mathcal{G}}_{\text{n,reg}}(\mathbf{X}_\ell; \mathbf{X}_\ell) - 2\pi n_\ell \nabla \overline{\mathcal{G}}_{\text{d,reg}}(\mathbf{X}_\ell; \mathbf{X}_\ell) \\ &\quad + 2\pi \tan(q \log \epsilon) \sum_{j=1, j \neq \ell}^N \nabla^\perp \overline{\mathcal{G}}_\text{n}(\mathbf{X}_\ell; \mathbf{X}_j) \\ &\quad - 2\pi \sum_{j=1, j \neq \ell}^N n_j \nabla \overline{\mathcal{G}}_\text{d}(\mathbf{X}_\ell; \mathbf{X}_j) \end{aligned} \quad (66)$$

As the size of the domain tends to infinity both the Neumann and Dirichlet Green's functions tend to

$$\frac{1}{2\pi} \log |\mathbf{X} - \mathbf{Y}|.$$

Equation (65) then becomes

$$\frac{\tilde{\mu}}{2} \tan(qn_\ell \log \epsilon) \frac{d\mathbf{X}_\ell}{dT} = \sum_{j=1, j \neq \ell}^N \frac{n_j \tan(qn_j \log \epsilon)}{|\mathbf{X}_\ell - \mathbf{X}_j|} \mathbf{e}_{\phi_j} + \sum_{j=1, j \neq \ell}^N \frac{n_j}{|\mathbf{X}_\ell - \mathbf{X}_j|} \mathbf{e}_{r_j}$$

in agreement with [2].

4 Rectangular domains

In this section we evaluate our results for a rectangular domain with sides of length L_x and L_y , in preparation for a comparison with direct numerical simulations in §5. As we have shown in the previous sections, we find two different laws of motion for spirals depending on the relative sizes of the domain and the parameter q . We first evaluate these two laws of motion for the case of a rectangle, before formulating a uniform approximation valid in both regimes.

4.1 Canonical scale

For spirals in a rectangular domain in which $L_x, L_y \sim 1/\epsilon \sim e^{\pi/2q}$ the motion takes place in the canonical scaling. Recalling that the outer variable is defined as $\mathbf{X} = \epsilon \mathbf{x}$, equation (13) for the Neumann Green's function $G_n(\mathbf{X}; \hat{\mathbf{X}})$ for the modified Helmholtz equation is, in this case

$$\begin{aligned} \nabla^2 G_n - \alpha^2 G_n &= \delta(\mathbf{X} - \hat{\mathbf{X}}) \quad \text{in} \quad [0, \epsilon L_x] \times [0, \epsilon L_y], \\ \frac{\partial G_n}{\partial X} &= 0 \quad \text{on} \quad X = 0 \text{ and } X = \epsilon L_x, \\ \frac{\partial G_n}{\partial Y} &= 0 \quad \text{on} \quad Y = 0 \text{ and } Y = \epsilon L_y, \end{aligned}$$

where $\mathbf{X} = (X, Y)$ and $\hat{\mathbf{X}} = (\hat{X}, \hat{Y})$. Using the method of images, and noting that the free space Green's function is given by (43), the solution is

$$\begin{aligned} G_n(\mathbf{X}; \hat{\mathbf{X}}) &= -\frac{1}{2\pi} \sum_{m,n=-\infty}^{\infty} K_0 \left(\alpha \left((X - \hat{X} + 2n\epsilon L_x)^2 + (Y - \hat{Y} + 2m\epsilon L_y)^2 \right)^{1/2} \right) \\ &\quad - \frac{1}{2\pi} \sum_{m,n=-\infty}^{\infty} K_0 \left(\alpha \left((X + \hat{X} + 2n\epsilon L_x)^2 + (Y - \hat{Y} + 2m\epsilon L_y)^2 \right)^{1/2} \right) \\ &\quad - \frac{1}{2\pi} \sum_{m,n=-\infty}^{\infty} K_0 \left(\alpha \left((X - \hat{X} + 2n\epsilon L_x)^2 + (Y + \hat{Y} + 2m\epsilon L_y)^2 \right)^{1/2} \right) \\ &\quad - \frac{1}{2\pi} \sum_{m,n=-\infty}^{\infty} K_0 \left(\alpha \left((X + \hat{X} + 2n\epsilon L_x)^2 + (Y + \hat{Y} + 2m\epsilon L_y)^2 \right)^{1/2} \right). \end{aligned}$$

The series are rapidly convergent since $K_0(z)$ decays exponentially for large z . We also defined the regular part of the Green's function by

$$G_{n,\text{reg}}(\mathbf{X}; \hat{\mathbf{X}}) = G_n(\mathbf{X}; \hat{\mathbf{X}}) - \frac{1}{2\pi} \log |\mathbf{X} - \hat{\mathbf{X}}|.$$

In order to compare with direct numerical simulation, we rewrite G_n in terms of the original variable \mathbf{x} by setting

$$\begin{aligned} G'_n(\mathbf{x}; \boldsymbol{\xi}) = G_n(\epsilon \mathbf{x}; \epsilon \boldsymbol{\xi}) &= -\frac{1}{2\pi} \sum_{m,n=-\infty}^{\infty} K_0 \left(qk \left((x - \xi + 2nL_x)^2 + (y - \eta + 2mL_y)^2 \right)^{1/2} \right) \\ &\quad - \frac{1}{2\pi} \sum_{m,n=-\infty}^{\infty} K_0 \left(qk \left((x + \xi + 2nL_x)^2 + (y - \eta + 2mL_y)^2 \right)^{1/2} \right) \\ &\quad - \frac{1}{2\pi} \sum_{m,n=-\infty}^{\infty} K_0 \left(qk \left((x - \xi + 2nL_x)^2 + (y + \eta + 2mL_y)^2 \right)^{1/2} \right) \\ &\quad - \frac{1}{2\pi} \sum_{m,n=-\infty}^{\infty} K_0 \left(qk \left((x + \xi + 2nL_x)^2 + (y + \eta + 2mL_y)^2 \right)^{1/2} \right), \end{aligned}$$

where $\hat{\mathbf{X}} = \epsilon \boldsymbol{\xi} = \epsilon(\xi, \eta)$, and we have written $\epsilon\alpha = qk$. Then

$$G'_{n,\text{reg}}(\mathbf{x}; \boldsymbol{\xi}) = G'_n(\mathbf{x}; \boldsymbol{\xi}) - \frac{1}{2\pi} \log |\mathbf{x} - \boldsymbol{\xi}| = G_{n,\text{reg}}(\epsilon \mathbf{x}; \epsilon \boldsymbol{\xi}) + \frac{1}{2\pi} \log \epsilon.$$

With a single spiral. In the particular case where there is only one spiral at position \mathbf{X}_1 with unitary winding number n_1 , the law of motion simply reads

$$\frac{d\mathbf{X}_1}{dT} = \frac{4\pi q n_1}{\mu} \nabla^\perp G_{n,\text{reg}}(\mathbf{X}_1; \mathbf{X}_1), \quad (67)$$

and α is given by

$$-2\pi G_{n,\text{reg}}(\mathbf{X}_1; \mathbf{X}_1) + c_1 + \log(1/\epsilon) - \pi/2q = 0. \quad (68)$$

Written in terms of the original variables \mathbf{x} , t and k equation (67) becomes

$$\frac{d\mathbf{x}_1}{dt} = 4\pi q n_1 \nabla^\perp G'_{n,\text{reg}}(\mathbf{x}_1; \mathbf{x}_1) \quad (69)$$

where ∇ now represents the gradient with respect to \mathbf{x} . Equation (68) becomes

$$-2\pi G'_{n,\text{reg}}(\mathbf{x}_1; \mathbf{x}_1) + c_1 - \pi/2q = 0.$$

Note that neither of these equations depends on the scaling parameters ϵ or μ , as expected.

With two spirals Written in terms of the original coordinate \mathbf{x} , with spirals at positions \mathbf{x}_1 and \mathbf{x}_2 , (40) gives

$$\begin{aligned} 2\pi\beta_1 G'_{n,\text{reg}}(\mathbf{x}_1; \mathbf{x}_1) + 2\pi\beta_2 G'_n(\mathbf{x}_1; \mathbf{x}_2) - \beta_1(c_1 - \pi/2q) &= 0, \\ 2\pi\beta_2 G'_{n,\text{reg}}(\mathbf{x}_2; \mathbf{x}_2) + 2\pi\beta_1 G'_n(\mathbf{x}_2; \mathbf{x}_1) - \beta_2(c_1 - \pi/2q) &= 0. \end{aligned}$$

The equation for k is thus

$$(-2\pi G'_{n,\text{reg}}(\mathbf{x}_1; \mathbf{x}_1) + c_1 - \pi/2q) (-2\pi G'_{n,\text{reg}}(\mathbf{x}_2; \mathbf{x}_2) + c_1 - \pi/2q) = 4\pi^2 G'_n(\mathbf{x}_2; \mathbf{x}_1) G'_n(\mathbf{x}_1; \mathbf{x}_2),$$

while

$$\frac{\beta_2}{\beta_1} = \frac{2\pi G'_{n,\text{reg}}(\mathbf{x}_1; \mathbf{x}_1) - c_1 + \pi/2q}{2\pi G'_n(\mathbf{x}_1; \mathbf{x}_2)} = \frac{2\pi G'_n(\mathbf{x}_2; \mathbf{x}_1)}{2\pi G'_{n,\text{reg}}(\mathbf{x}_2; \mathbf{x}_2) - c_1 + \pi/2q}.$$

Note that $G'_n(\mathbf{x}_2; \mathbf{x}_1) = G'_n(\mathbf{x}_1; \mathbf{x}_2)$.

Written in terms of the original variables \mathbf{x} and t the law of motion (67) for two spirals is

$$\begin{aligned} \frac{d\mathbf{x}_1}{dt} &= 4\pi q n_1 \frac{\beta_2}{\beta_1} \nabla^\perp G'_n(\mathbf{x}_1; \mathbf{x}_2) + 4\pi q n_1 \nabla^\perp G'_{n,\text{reg}}(\mathbf{x}_1; \mathbf{x}_1) \\ \frac{d\mathbf{x}_2}{dt} &= 4\pi q n_2 \frac{\beta_1}{\beta_2} \nabla^\perp G'_n(\mathbf{x}_2; \mathbf{x}_1) + 4\pi q n_2 \nabla^\perp G'_{n,\text{reg}}(\mathbf{x}_2; \mathbf{x}_2). \end{aligned}$$

Remark 1 We note that if initially $\mathbf{x}_1 + \mathbf{x}_2 = (L_x, L_y)$, so that the spirals are placed symmetrically with respect to the centre of the domain, then if $n_1 = n_2$ they keep this symmetry during the motion. In this case $G'_{n,\text{reg}}(\mathbf{x}_1; \mathbf{x}_1) = G'_{n,\text{reg}}(\mathbf{x}_2; \mathbf{x}_2)$ so that $\beta_2/\beta_1 = 1$.

4.2 Near-field scale

In the near field scaling the relevant Green's functions are the Neumann and Dirichlet Green's functions for Laplace's equation. We rewrite these in the original variables as $\overline{G}'_n(\mathbf{x}; \boldsymbol{\xi}) = \overline{G}'_n(\epsilon\mathbf{x}; \epsilon\boldsymbol{\xi})$, $\overline{G}'_d(\mathbf{x}; \boldsymbol{\xi}) = \overline{G}'_d(\epsilon\mathbf{x}; \epsilon\boldsymbol{\xi})$. As before, we evaluate the Green's functions by the method of images. However, we must be a little careful, because the sums over images for the Green's functions themselves do not converge. However, the corresponding sums over images for the

derivatives of the Green's functions do converge, and these are what we need for the law of motion. Defining

$$\begin{aligned}
V_x(\mathbf{x}; \xi, \eta) &= \frac{1}{2\pi} \sum_{n,m=-\infty}^{\infty} \frac{x - \xi + 2L_x n}{(x - \xi + 2nL_x)^2 + (y - \eta + 2mL_y)^2} \\
&= \frac{1}{2\pi} \sum_{m=-\infty}^{\infty} \frac{\pi \sin(\pi(x - \xi)/L_x)}{2L_x (\cosh(\pi((y - \eta) + 2L_y m)/L_x) - \cos(\pi(x - \xi)/L_x))}, \\
V_y(\mathbf{x}; \xi, \eta) &= \frac{1}{2\pi} \sum_{n,m=-\infty}^{\infty} \frac{y - \eta + 2L_y m}{(x - \xi + 2nL_x)^2 + (y - \eta + 2mL_y)^2} \\
&= \frac{1}{2\pi} \sum_{n=-\infty}^{\infty} \frac{\pi \sin(\pi(y - \eta)/L_y)}{2L_y (\cosh(\pi((x - \xi) + 2L_x n)/L_y) - \cos(\pi(y - \eta)/L_y))},
\end{aligned}$$

then

$$\begin{aligned}
\frac{\partial \bar{G}'_n}{\partial x}(\mathbf{x}; \xi) &= V_x(\mathbf{x}; \xi, \eta) + V_x(\mathbf{x}; -\xi, \eta) + V_x(\mathbf{x}; \xi, -\eta) + V_x(\mathbf{x}; -\xi, -\eta), \\
\frac{\partial \bar{G}'_n}{\partial y}(\mathbf{x}; \xi) &= V_y(\mathbf{x}; \xi, \eta) + V_y(\mathbf{x}; -\xi, \eta) + V_y(\mathbf{x}; \xi, -\eta) + V_y(\mathbf{x}; -\xi, -\eta), \\
\frac{\partial \bar{G}'_d}{\partial x}(\mathbf{x}; \xi) &= V_x(\mathbf{x}; \xi, \eta) - V_x(\mathbf{x}; -\xi, \eta) - V_x(\mathbf{x}; \xi, -\eta) + V_x(\mathbf{x}; -\xi, -\eta), \\
\frac{\partial \bar{G}'_d}{\partial y}(\mathbf{x}; \xi) &= V_y(\mathbf{x}; \xi, \eta) - V_y(\mathbf{x}; -\xi, \eta) - V_y(\mathbf{x}; \xi, -\eta) + V_y(\mathbf{x}; -\xi, -\eta).
\end{aligned}$$

Note that the final sums above again converge exponentially quickly. In terms of \mathbf{x} and t the law of motion is

$$\begin{aligned}
\frac{n_\ell}{2q} \tan(q \log \epsilon) \frac{d\mathbf{x}_\ell}{dt} &= 2\pi \tan(q \log \epsilon) \nabla^\perp \bar{G}'_{n,\text{reg}}(\mathbf{x}_\ell; \mathbf{x}_\ell) - 2\pi n_\ell \nabla \bar{G}'_{d,\text{reg}}(\mathbf{x}_\ell; \mathbf{x}_\ell) \\
&\quad + 2\pi \tan(q \log \epsilon) \sum_{j=1, j \neq \ell}^N \nabla^\perp \bar{G}'_n(\mathbf{x}_\ell; \mathbf{x}_j) - 2\pi \sum_{j=1, j \neq \ell}^N n_j \nabla \bar{G}'_d(\mathbf{x}_\ell; \mathbf{x}_j). \quad (70)
\end{aligned}$$

Recall also that

$$k = \left(\frac{2\pi N}{q|\Omega|} \tan(q \log(1/\epsilon)) \right)^{1/2},$$

where $|\Omega|$ is the area of Ω in the original variable \mathbf{x} .

With a single spiral Written out in component form, the law of motion for a single spiral at \mathbf{x}_1 with winding number $|n_1| = 1$ is

$$\begin{aligned}
\frac{dx_1}{dt} &= -4\pi q n_1 \frac{\partial \bar{G}'_{n,\text{reg}}(\mathbf{x}_1; \mathbf{x}_1)}{\partial y} - 4\pi q \cot(q \log \epsilon) \frac{\partial \bar{G}'_{d,\text{reg}}(\mathbf{x}_1; \mathbf{x}_1)}{\partial x}, \\
\frac{dy_1}{dt} &= 4\pi q n_1 \frac{\partial \bar{G}'_{n,\text{reg}}(\mathbf{x}_1; \mathbf{x}_1)}{\partial x} - 4\pi q \cot(q \log \epsilon) \frac{\partial \bar{G}'_{d,\text{reg}}(\mathbf{x}_1; \mathbf{x}_1)}{\partial y}.
\end{aligned}$$

With two spirals Written out in component form, the law of motion for spirals at positions \mathbf{x}_1 and \mathbf{x}_2 with winding numbers $|n_1| = |n_2| = 1$ is

$$\begin{aligned}
\frac{dx_1}{dt} &= -4\pi q n_1 \frac{\partial \overline{G}'_{n,\text{reg}}(\mathbf{x}_1; \mathbf{x}_1)}{\partial y} - 4\pi q \cot(q \log \epsilon) \frac{\partial \overline{G}'_{d,\text{reg}}(\mathbf{x}_1; \mathbf{x}_1)}{\partial x} \\
&\quad - 4\pi q n_1 \frac{\partial \overline{G}'_n(\mathbf{x}_1; \mathbf{x}_2)}{\partial y} - 4\pi q n_2 n_1 \cot(q \log \epsilon) \frac{\partial \overline{G}'_d(\mathbf{x}_1; \mathbf{x}_2)}{\partial x}, \\
\frac{dy_1}{dt} &= 4\pi q n_1 \frac{\partial \overline{G}'_{n,\text{reg}}(\mathbf{x}_1; \mathbf{x}_1)}{\partial x} - 4\pi q \cot(q \log \epsilon) \frac{\partial \overline{G}'_{d,\text{reg}}(\mathbf{x}_1; \mathbf{x}_1)}{\partial y} \\
&\quad + 4\pi n_1 q \frac{\partial \overline{G}'_n(\mathbf{x}_1; \mathbf{x}_2)}{\partial x} - 4\pi q n_1 n_2 \cot(q \log \epsilon) \frac{\partial \overline{G}'_d(\mathbf{x}_1; \mathbf{x}_2)}{\partial y}, \\
\frac{dx_2}{dt} &= -4\pi n_2 q \frac{\partial \overline{G}'_{n,\text{reg}}(\mathbf{x}_2; \mathbf{x}_2)}{\partial y} - 4\pi q \cot(q \log \epsilon) \frac{\partial \overline{G}'_{d,\text{reg}}(\mathbf{x}_2; \mathbf{x}_2)}{\partial x} \\
&\quad - 4\pi q n_2 \frac{\partial \overline{G}'_n(\mathbf{x}_2; \mathbf{x}_1)}{\partial y} - 4\pi q n_1 n_2 \cot(q \log \epsilon) \frac{\partial \overline{G}'_d(\mathbf{x}_2; \mathbf{x}_1)}{\partial x}, \\
\frac{dy_2}{dt} &= 4\pi q n_2 \frac{\partial \overline{G}'_{n,\text{reg}}(\mathbf{x}_2; \mathbf{x}_2)}{\partial x} - 4\pi q \cot(q \log \epsilon) \frac{\partial \overline{G}'_{d,\text{reg}}(\mathbf{x}_2; \mathbf{x}_2)}{\partial y} \\
&\quad + 4\pi q n_2 \frac{\partial \overline{G}'_n(\mathbf{x}_2; \mathbf{x}_1)}{\partial x} - 4\pi q n_1 n_2 \cot(q \log \epsilon) \frac{\partial \overline{G}'_d(\mathbf{x}_2; \mathbf{x}_1)}{\partial y}.
\end{aligned}$$

4.3 A uniform composite expansion

To compare with direct numerical simulations we combine the expansions of Sections 4.1 and 4.2 into a single composite expansion valid in both regions. We first consider the asymptotic wavenumber. As $\alpha \rightarrow 0$ in (41) we find

$$G_n(\mathbf{X}; \mathbf{Y}) \sim -\frac{1}{|\overline{\Omega}| \alpha^2} + \overline{G}_n(\mathbf{X}; \mathbf{Y}) + \dots,$$

where $\overline{G}_n(\mathbf{X}; \mathbf{Y})$ is the Neumann Green's function for Laplace's equation given by (50). Thus (40) implies that the β_ℓ are all equal to leading order and α is given by

$$\alpha^2 \sim \frac{2\pi N q}{|\overline{\Omega}|(\pi/2 - q|\log \epsilon|)}.$$

We see that this matches smoothly into the near-field α we found in (61), since

$$\alpha^2 = q \tilde{\alpha}^2 = \frac{2\pi q N}{|\overline{\Omega}|} \tan(q \log(1/\epsilon)) \sim \frac{2\pi N q}{|\overline{\Omega}|(\pi/2 - q|\log \epsilon|)}$$

as $q|\log \epsilon| \rightarrow \pi/2$. We may generate a uniform approximation to α by taking

$$\alpha^2 = \alpha_{\text{canonical}}^2 + \alpha_{\text{near}}^2 - \frac{2\pi N q}{|\overline{\Omega}|(\pi/2 - q|\log \epsilon|)}.$$

The corresponding uniform approximation to k is given by

$$k^2 = k_{\text{canonical}}^2 + \frac{2\pi N}{q|\overline{\Omega}|} \tan(q \log(1/\epsilon)) - \frac{2\pi N}{q|\overline{\Omega}|(\pi/2 - q|\log \epsilon|)}. \quad (71)$$

For the law of motion the simplest uniformly valid composite expansion is

$$\begin{aligned} \frac{d\mathbf{x}_\ell}{dt} = & \frac{4\pi q n_\ell}{\beta_\ell} \sum_{j=1, j \neq \ell}^N \beta_j \nabla^\perp G'_n(\mathbf{x}_\ell; \mathbf{x}_j) + 4\pi q n_\ell \nabla^\perp G'_{n,\text{reg}}(\mathbf{x}_\ell; \mathbf{x}_\ell) \\ & - 4\pi q \cot(q \log \epsilon) \nabla G'_{d,\text{reg}}(\mathbf{x}_\ell; \mathbf{x}_\ell) - \frac{4\pi q \cot(q \log \epsilon)}{n_\ell} \sum_{j=1, j \neq \ell}^N n_j \nabla G'_d(\mathbf{x}_\ell; \mathbf{x}_j), \end{aligned} \quad (72)$$

where G'_d is the Dirichlet Green's function for the modified Helmholtz equation given by

$$\nabla^2 G'_d - q^2 k^2 G'_d = \delta(\mathbf{x} - \mathbf{y}) \quad \text{in } \Omega, \quad G'_d = 0 \quad \text{on } \partial\Omega, \quad (73)$$

with

$$G'_{d,\text{reg}}(\mathbf{x}; \mathbf{y}) = G'_d(\mathbf{x}; \mathbf{y}) - \frac{1}{2\pi} \log |\mathbf{x} - \mathbf{y}|,$$

and β_ℓ and k are given by the canonical approximation in §4.1.

4.4 Choice of ϵ

In order to plot the trajectories obtained from the uniformly valid asymptotic approximation to the law of motion we need to make one final choice as to the value of ϵ , which is the inverse of the typical separation between spirals (and their images). In principle, the full asymptotic expansion is independent of ϵ when written in the original coordinates (note that ϵ disappears from the approximation for k in the canonical region, for example, when it is rewritten in the original variables)—this is reflected in the law of motion by the fact that ϵ only appears as $\log \epsilon$: multiplying ϵ by any factor does not change the law of motion asymptotically. However, ϵ will only disappear from the near-field (and uniform) law of motion if we include the full expansion to all powers of $\log \epsilon$ (i.e. all powers of q). Since this is not possible, we must choose an appropriate lengthscale to use for ϵ . In principle any choice will do (all lead to the same law of motion at leading order).

In our numerical comparisons we consider two natural choices for ϵ . The first is simply to choose ϵ to be a constant proportional to the inverse of the domain diameter—we take $\epsilon = 4/(L_x + L_y)$, which is 0.01 for the square domain of side length 200 we consider in §5. The second natural choice is to take ϵ to be proportional to the inverse distance from a spiral to the boundary or between spirals. For a single spiral at (x_1, y_1) we approximate this by setting

$$\epsilon = \left(\frac{1}{x_1^2} + \frac{1}{|L_x - x_1|^2} + \frac{1}{y_1^2} + \frac{1}{|L_y - y_1|^2} \right)^{1/2}. \quad (74)$$

For two spirals at (x_1, y_1) and $(L_x - x_1, L_y - y_1)$ we take

$$\epsilon = \left(\frac{1}{x_1^2} + \frac{1}{|L_x - x_1|^2} + \frac{1}{y_1^2} + \frac{1}{|L_y - y_1|^2} + \frac{1}{|L_x/2 - x_1|^2 + |L_y/2 - y_1|^2} \right)^{1/2}. \quad (75)$$

5 Comparison with direct numerical simulations

To test the accuracy of our results, numerical simulations were carried out for the Neumann problem. Letting $\psi(x, y, t) = e^{-ik^2 q t} \hat{\psi}(x, y, t)$, equation (5) becomes

$$\hat{\psi}_t = (1 + iq)(1 - |\hat{\psi}|^2)\hat{\psi} + \nabla^2 \hat{\psi} \quad \text{in } \Omega, \quad \frac{\partial \hat{\psi}}{\partial n} = 0 \quad \text{on } \partial\Omega, \quad (76)$$

Numerical simulations of equation (76) were carried out using finite differences applied to the coupled reaction-diffusion equations for the real and imaginary parts of $\hat{\psi}$ subject to homogeneous Neumann boundary conditions on a large square domain. A uniform spatial discretization was used with $\Delta y = \Delta x$. Following the approach described in [8, 5], a nine-point stencil for the Laplacian operator was used to obtain more accurate approximations of the oscillating solutions. Explicit timestepping using Euler's method with a small timestep, $\Delta t = (\Delta x)^2/20$, was found to be stable and computationally efficient.

Initial conditions were chosen to have zeros with a unit winding number at the desired initial location of the spirals. In particular, for a single spiral, initial data at $t = 0$ was chosen as

$$\hat{\psi}_0(\mathbf{x}) = \hat{f}(r_1)e^{i\hat{\chi}(r_1, \theta_1)}$$

where (r_1, θ_1) are polar coordinates with respect to the intended starting position, \mathbf{x}_1 , for the centre of the spiral, $\hat{f}(r) = \tanh(Ar)$ where $A = 0.583189$ was chosen to match $\hat{f}'(0)$ with the solution for a steady spiral in an infinite domain [11], and the phase $\hat{\chi}$ varies by 2π as \mathbf{x}_1 is circled anticlockwise. Since the leading-order equation for the phase in the outer region ((9) and (48) respectively in the canonical and near-field scalings) is quasi-steady, in principle any such initial condition $\hat{\chi}$ will do, since χ will equilibrate over a short timescale. However, since the timescale for evolution of χ is only logarithmically smaller (i.e. $O(1/|\log \epsilon|)$) than that for the motion of spirals, in practice initial transients in χ can significantly perturb the motion. To eliminate this as much as possible we choose the initial $\hat{\chi}$ to be given by either the near-field χ_{01} corresponding to the initial position of the spiral (the solution of (48)) or the canonical $\theta_1 + \chi_{00}/q$ corresponding to the initial position of the spiral (where χ_{00} is the solution of (9)). In the near-field this requires us to choose a value of ϵ ; we take $\epsilon = 0.01$ for simplicity.

For pairs of spirals starting at \mathbf{x}_1 and \mathbf{x}_2 , the initial condition was given as

$$\hat{\psi}_0(\mathbf{x}) = \hat{f}(r_1)\hat{f}(r_2)\exp(i[\hat{\chi}(r_1, \theta_1) + \hat{\chi}(r_2, \theta_2)]).$$

It was observed that this choice of initial data led to brief transients after which $\hat{\psi}$ was smooth, slowly-evolving and satisfied the boundary conditions. For the most part the transients caused only relatively small changes to the starting positions \mathbf{x}_i of the spirals. However, when the near-field initial condition for χ was used with too large a value of q (in which $q|\log \epsilon|$ is too close to $\pi/2$) it was observed that many more zeros of ψ were generated locally during the initial transient, and that these additional spirals did not always annihilate with each other. We used this behaviour to determine when to switch from the near-field initial condition to the canonical initial condition: for a single spiral we use the near-field initial condition for $q \leq 0.3$ and the canonical initial condition for $q \geq 0.35$; for two spirals we use the near-field initial condition for $q \leq 0.2$ canonical initial condition for $q \geq 0.25$. Figure 1 shows a snapshot of the real and imaginary parts and the phase of $\hat{\psi}$ for an example with two spirals.

In order to compare the simulations with the asymptotic predictions we need to calculate the trajectories of the spiral centres, $\mathbf{x}_i(t)$. From the simulations, at regularly spaced times, t_j , the positions of local minima of $|\psi|$ were interpolated to sub-grid resolution by fitting computed values at grid points surrounding the discrete minimum to a paraboloid. In Figure 2 we show some examples of the trajectories obtained from this procedure, for a single +1 spiral with various starting positions. This figure illustrates the effect that the initial condition on the phase χ can have on the trajectory of the spiral. It also illustrates a difficulty we will have when comparing our asymptotic trajectories to the numerically determined trajectories: because trajectories from nearby initial conditions are diverging, any small differences in the velocities will be compounded over time so that small errors in velocity may lead to large errors in position and quite different paths.

In Figure 3 we show a comparison between the numerically determined velocity (by finite differencing the numerically determined path in time) and the velocity predicted by the uniform asymptotic approximation described above, as a function of time along the numerically determined spiral trajectory. The numerical solutions are for a single +1 spiral in the square domain $0 \leq x, y \leq 200$ with grid resolution $\Delta x = 0.5$. For each value of q the x and y velocities for two different trajectories (i.e. two different starting positions) are shown. The asymptotic results are shown for the two choices of ϵ described in §4.4. We see that there are still some initial transients in the velocities, but that on the whole the asymptotic approximation does quite well. The approximation gets better as q increases, which seems slightly counter-intuitive since the asymptotic approximation is in the limit $q \rightarrow 0$. This can be explained by the fact that in the near-field scaling the $1/\log \epsilon$ correction terms play a more significant role than they do in the canonical scaling (in the canonical region ϵ disappears from the law of motion when written in terms of the original variables, while in the near field region it does not). From Figure 3 we also see that the green curves, corresponding to choosing $\epsilon = 0.01$, fit less well at higher values of q , particularly near the end of the trajectory in which the spiral is approaching the boundary. On the other hand the blue curves, which take the distance to the boundary into account in ϵ through (74), fit very well.

In Figure 4 we compare directly the numerical trajectories (dashed lines) and those given by the uniform asymptotic approximation with ϵ given by (74) (solid lines), for a single +1 spiral in a square domain $0 \leq x, y \leq 200$. Numerical trajectories are shown starting from positions $(110, 100), (120, 100), \dots, (170, 100)$. Because of the initial transients in the numerical results, and to mitigate the effects of diverging trajectories mentioned earlier, we solve the asymptotic trajectories backwards from a point on the numerical trajectory near the boundary of the domain². Specifically we find the asymptotic trajectory which meets the numerical trajectory on curve $(x - 100)^4 + (y - 100)^4 = 90^4$.

For small q we see that the spiral is attracted to the boundary whatever its initial position. However, as q is increased there is a Hopf bifurcation with the appearance of an unstable periodic orbit. Trajectories starting outside this periodic orbit are attracted to the boundary of the domain, but those starting inside it spiral in to the origin. As q is increased further the periodic orbit grows in size and develops a more squareish shape. This can be understood as the spiral interacting with its images predominantly in the near-field limit, in which the motion is perpendicular to the line of centres. With the motion dominated by the nearest image the spiral will move parallel to the nearest boundary until it nears the corner, when a second image takes over. We see that the asymptotic law of motion captures the appearance of the periodic orbit. In Fig. 4e the amplitude of the asymptotic periodic orbit is not quite right (it crosses the line $y = 100$ close to $x = 110$ rather than $x = 130$), but in Fig. 4f the periodic orbit is captured well quantitatively as well as qualitatively.

In Figure 5 we compare the trajectories provided by a direct numerical simulation of (5) (dashed lines) and those given by the uniform asymptotic approximation (solid lines) for a pair of +1 spirals in the same square domain $0 \leq x, y \leq 200$. We position the spirals symmetrically at positions $(100 - x, 100)$ and $(100 + x, 100)$, where we choose $x = 10, 20, \dots, 70$. As in Figure 4, the asymptotic trajectories are those which meet the numerical trajectory on curve $(x - 100)^4 + (y - 100)^4 = 90^4$. We see that the agreement is qualitatively very good, again improving as q increases. The spirals attempt to circle around each other, as the near-field interaction would indicate, but gradually drift apart until the image spirals take over and force the pair to rotate in the opposite direction.

²For trajectories which do not leave the domain we solve forwards from the initial position.

6 Conclusions

We have developed a law of motion for interacting spiral waves in a bounded domain in the limit that the twist parameter q is small. We find that the size of the domain is crucial in determining the form of this law of motion. Our main results can be summarised as follows. For $0 < q \ll 1$, given a set of ± 1 -armed spirals in a domain of diameter $O(1/\epsilon)$, the positions \mathbf{x}_ℓ of the spirals evolve according to the following laws of motion:

- (i) For a so-called *canonical* domain size, which corresponds to $q|\log \epsilon| = \pi/2 + q\nu$ with $\nu = O(1)$ as $q, \epsilon \rightarrow 0$,

$$\frac{d\mathbf{x}_\ell}{dt} = \frac{4\pi q n_\ell}{\beta_\ell} \sum_{j=1, j \neq \ell}^N \beta_j \nabla^\perp G'_n(\mathbf{x}_\ell; \mathbf{x}_j) + 4\pi q n_\ell \nabla^\perp G'_{n,\text{reg}}(\mathbf{x}_\ell; \mathbf{x}_\ell) \quad (77)$$

where $\nabla^\perp = (-\partial_y, \partial_x)$ and $G'_n(\mathbf{x}; \mathbf{y})$ is the Neumann Green's function for the modified Helmholtz equation on Ω , satisfying

$$\nabla^2 G'_n - q^2 k^2 G'_n = \delta(\mathbf{x} - \mathbf{y}) \quad \text{in } \Omega, \quad \frac{\partial G'_n}{\partial n} = 0 \quad \text{on } \partial\Omega. \quad (78)$$

with

$$G'_{n,\text{reg}}(\mathbf{x}; \mathbf{y}) = G'_n(\mathbf{x}; \mathbf{y}) - \frac{1}{2\pi} \log |\mathbf{x} - \mathbf{y}|.$$

The coefficients β_ℓ are given (up to an arbitrary and irrelevant scaling factor) as solutions of the linear system of equations

$$2\pi \beta_\ell G'_{n,\text{reg}}(\mathbf{x}_\ell; \mathbf{x}_\ell) + 2\pi \sum_{j=1, j \neq \ell}^N \beta_j G'_n(\mathbf{x}_\ell; \mathbf{x}_j) - \beta_\ell (c_1 - \pi/2q) = 0, \quad (79)$$

where $c_1 \approx 0.098$, whose solvability condition (the condition for a non-zero solution) determines the eigenvalue k .

- (ii) For a so-called *near-field* domain size, which corresponds to $0 < q|\log \epsilon| < \pi/2$,

$$\begin{aligned} \frac{d\mathbf{x}_\ell}{dt} = & 4\pi q n_\ell \sum_{j=1, j \neq \ell}^N \nabla^\perp \overline{G}'_n(\mathbf{x}_\ell; \mathbf{x}_j) + 4\pi q n_\ell \nabla^\perp \overline{G}'_{n,\text{reg}}(\mathbf{x}_\ell; \mathbf{x}_\ell) \\ & - 4\pi q \cot(q \log \epsilon) \nabla \overline{G}'_{d,\text{reg}}(\mathbf{x}_\ell; \mathbf{x}_\ell) - \frac{4\pi q \cot(q \log \epsilon)}{n_\ell} \sum_{j=1, j \neq \ell}^N n_j \nabla \overline{G}'_d(\mathbf{x}_\ell; \mathbf{x}_j), \end{aligned} \quad (80)$$

where $\overline{G}'_n(\mathbf{x}; \mathbf{y})$ and $\overline{G}'_d(\mathbf{x}; \mathbf{y})$ are the Neumann and Dirichlet Green's functions for Laplace's equation on Ω , satisfying

$$\nabla^2 \overline{G}'_n = \delta(\mathbf{x} - \mathbf{y}) - \frac{1}{|\Omega|} \quad \text{in } \Omega, \quad \frac{\partial \overline{G}'_n}{\partial n} = 0 \quad \text{on } \partial\Omega, \quad (81)$$

$$\nabla^2 \overline{G}'_d = \delta(\mathbf{x} - \mathbf{y}) \quad \text{in } \Omega, \quad \overline{G}'_d = 0 \quad \text{on } \partial\Omega, \quad (82)$$

and

$$\overline{G}'_{n,\text{reg}}(\mathbf{x}; \mathbf{y}) = \overline{G}'_n(\mathbf{x}; \mathbf{y}) - \frac{1}{2\pi} \log |\mathbf{x} - \mathbf{y}|, \quad \overline{G}'_{d,\text{reg}}(\mathbf{x}; \mathbf{y}) = \overline{G}'_d(\mathbf{x}; \mathbf{y}) - \frac{1}{2\pi} \log |\mathbf{x} - \mathbf{y}|.$$

(iii) A uniform approximation, valid in both regions, is given by

$$\begin{aligned} \frac{d\mathbf{x}_\ell}{dt} = & \frac{4\pi q n_\ell}{\beta_\ell} \sum_{j=1, j \neq \ell}^N \beta_j \nabla^\perp G'_n(\mathbf{x}_\ell; \mathbf{x}_j) + 4\pi q n_\ell \nabla^\perp G'_{n,\text{reg}}(\mathbf{x}_\ell; \mathbf{x}_\ell) \\ & - 4\pi q \cot(q \log \epsilon) \nabla G'_{d,\text{reg}}(\mathbf{x}_\ell; \mathbf{x}_\ell) - \frac{4\pi q \cot(q \log \epsilon)}{n_\ell} \sum_{j=1, j \neq \ell}^N n_j \nabla G'_d(\mathbf{x}_\ell; \mathbf{x}_j), \end{aligned} \quad (83)$$

where G'_d is the Dirichlet Green's function for the modified Helmholtz equation given by

$$\nabla^2 G'_d - q^2 k^2 G'_d = \delta(\mathbf{x} - \mathbf{y}) \quad \text{in } \Omega, \quad G'_d = 0 \quad \text{on } \partial\Omega, \quad (84)$$

with

$$G'_{d,\text{reg}}(\mathbf{x}; \mathbf{y}) = G'_d(\mathbf{x}; \mathbf{y}) - \frac{1}{2\pi} \log |\mathbf{x} - \mathbf{y}|,$$

and β_ℓ and k given by (79).

Although we have focussed on Neumann boundary conditions for the complex Ginzburg-Landau equation (4), the extension to periodic boundary conditions is straightforward.

Acknowledgements M. Agualeles is part of the Catalan Research group 2017 SGR 1392 and has been supported by the MINECO grant MTM2017-84214-C2-2-P (Spain). She would also like to thank the Oxford Centre for Industrial and Applied Mathematics, where part of this research was carried out.

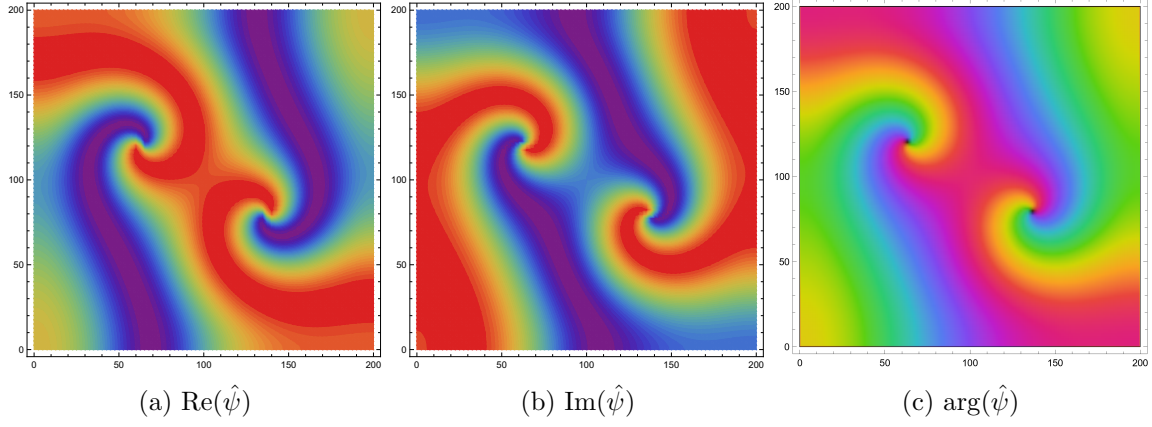


Figure 1: A snapshot of a simulation with two spirals for $q = 0.1$.

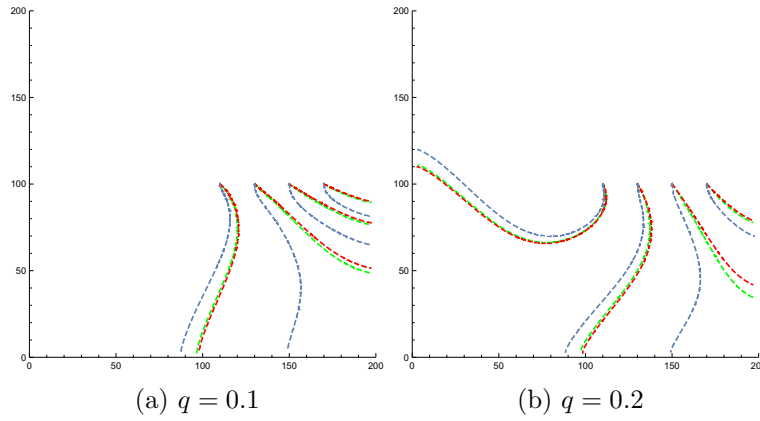


Figure 2: Numerically obtained trajectories for a single spiral starting at positions $y = 100$ and $x = 110, 130, 150$ and 170 . The different colours correspond to different initial conditions for the phase χ : blue is the canonical initial condition, red is the near-field initial condition with $\epsilon = 0.01$, and green is the near-field initial condition with $\epsilon = 0.005$.

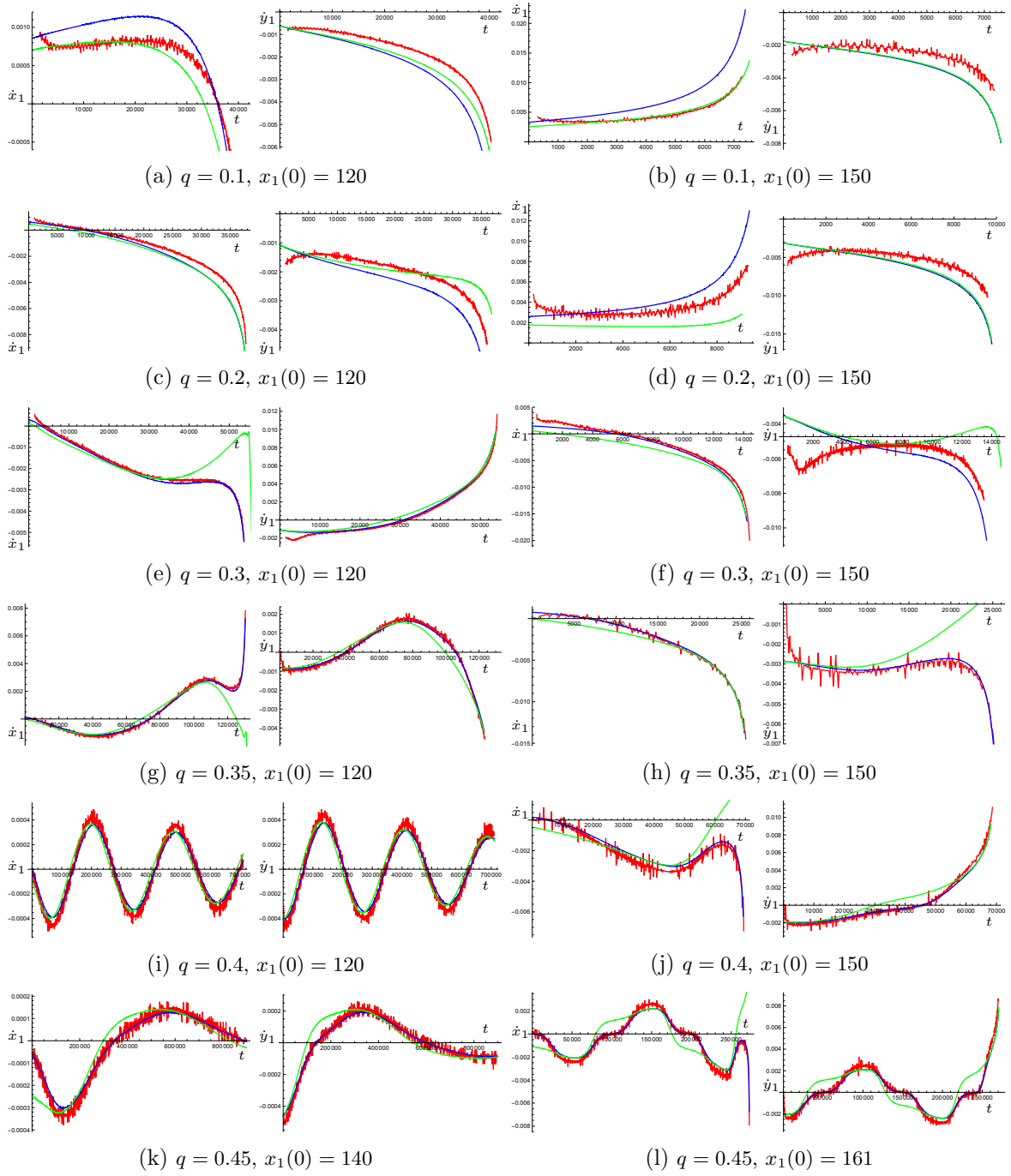


Figure 3: A comparison between the numerically determined velocity (red), the predicted asymptotic velocity with $\epsilon = 0.01$ (green), and the predicted asymptotic velocity with ϵ given by (74) (blue), as a function of time along the numerically determined spiral trajectory, for a single spiral in the square domain $[0, 200] \times [0, 200]$. For each value of q the x and y velocities for two different trajectories are shown, all of which have $y_1(0) = 100$. The numerical results have been locally averaged to reduce some of the noise. The trajectories themselves may be seen in Figure 4.

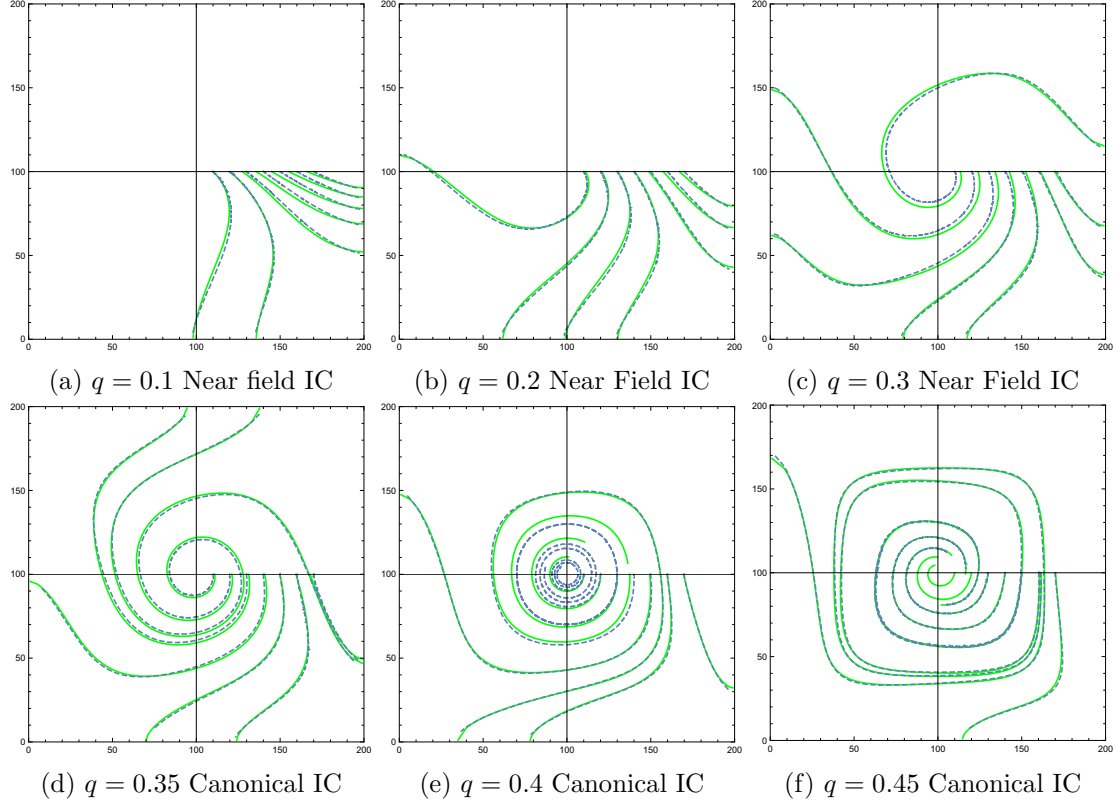


Figure 4: Comparison between the trajectories provided by a direct numerical simulation of (76) (dashed lines) and the uniform asymptotic approximation of §4.3 (solid lines) for a single spiral in a square domain of side 200. Numerical trajectories starting from positions $(110, 100), (120, 100), \dots, (170, 100)$ are shown; ϵ is given by (74). The asymptotic trajectories shown are those which meet the numerical trajectories on the curve $(x - 100)^4 + (y - 100)^4 = 90^4$ (apart from those which don't meet this curve, for which the numerical starting position is used). Note the appearance of an unstable periodic orbit in (e) and (f) which is captured by the asymptotic law of motion. An extra orbit starting from position $(161, 100)$ is shown in (f)—the periodic orbit crosses the line $x = 100$ somewhere between 160 and 161.

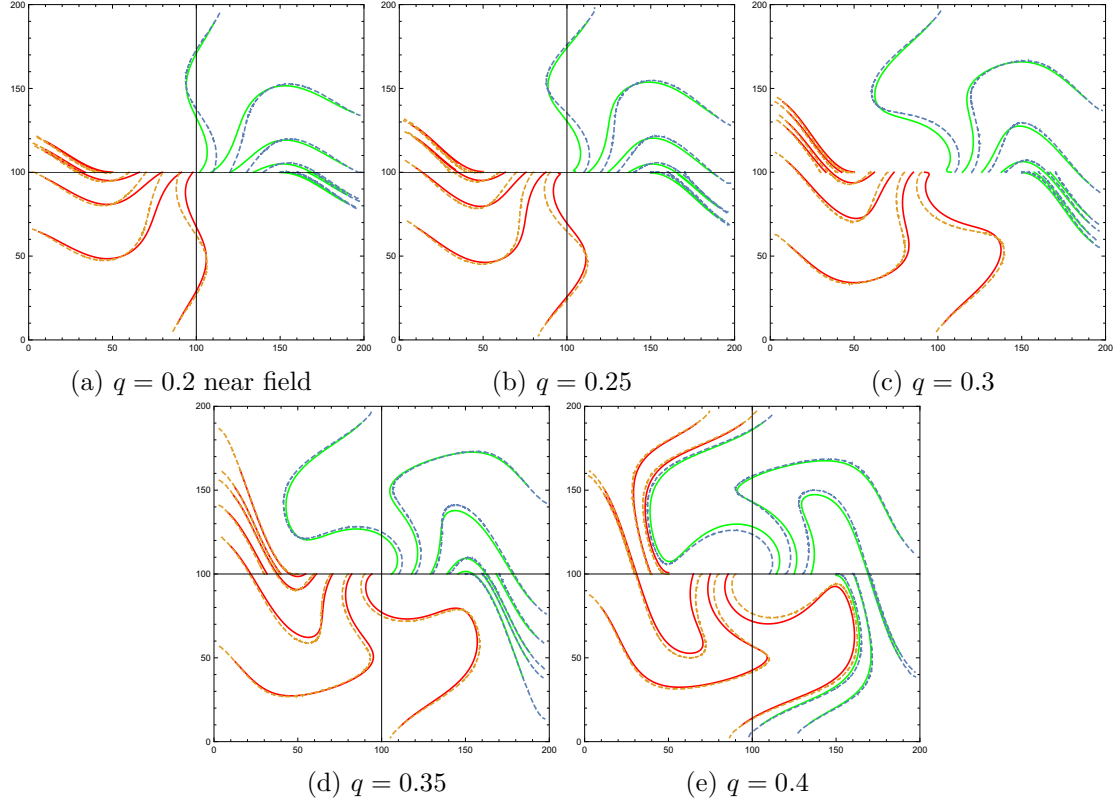


Figure 5: Comparison between the trajectories provided by a direct numerical simulation of (76) (dashed lines) and the uniform asymptotic approximation of §4.3 (solid lines) for a pair of spirals in a square domain of side 200. Spirals are placed symmetrically at positions $(100 - x, 100)$ and $(100 + x, 100)$ with $x = 10, 20, \dots, 70$; ϵ is given by (75). The asymptotic trajectories shown are those which meet the numerical trajectories on the curve $(x - 100)^4 + (y - 100)^4 = 90^4$.

References

- [1] M. Aguiar. The effect of boundaries on the asymptotic wavenumber of spiral wave solutions of the complex Ginzburg–Landau equation. *Phys. D*, 278:1–12, 2014.
- [2] M. Aguiar, S. J. Chapman, and T. Witelski. Interaction of Spiral Waves in the Complex Ginzburg–Landau Equation. *Phys. Rev. Lett.*, 101(22), Nov 28 2008.
- [3] M. Aguiar, S. J. Chapman, and T. Witelski. Motion of spiral waves in the complex Ginzburg–Landau equation. *Phys. D*, 239(7):348–365, 2010.
- [4] Igor S. Aranson and Lorenz Kramer. The world of the complex Ginzburg–Landau equation. *Rev. Mod. Phys.*, 74(1):99–143, 2002.
- [5] M. Barkley, M. Kness, and L.S. Tuckerman. Spiral-wave dynamics in a simple model of excitable media: the transition from simple to compound rotation. *Phys. Rev. A*, 42(4):2489–2492, 1990.
- [6] Tomas Bohr, Greg Huber, and Edward Ott. The structure of spiral-domain patterns and shocks in the 2D complex Ginzburg–Landau equation. *Phys. D*, 106(1-2):95–112, 1997.
- [7] Subir K Das. Unlocking of frozen dynamics in the complex Ginzburg–Landau equation. *Phys. Rev. E*, 87(1):012135, 2013.
- [8] M. Dowle, R. M. Mantel, and D. Barkley. Fast simulations of waves in three-dimensional excitable media. *Int. J. of Bif. and Chaos*, 7(11):2529–2545, 1997.
- [9] Milton Van Dyke. *Perturbation methods in fluid mechanics*. Academic Press, New York, 1964.
- [10] J.M. Greenberg. Spiral waves for $\lambda - \omega$ systems. *SIAM J. Appl. Math.*, 39(2): 536–547, 1980.
- [11] Patrick S. Hagan. Spiral waves in reaction-diffusion equations. *SIAM J. Appl. Math.*, 42(4):762–786, 1982.
- [12] PC Hohenberg and AP Krekhov. An introduction to the Ginzburg–Landau theory of phase transitions and nonequilibrium patterns. *Physics Reports*, 572:1–42, 2015.
- [13] Y. Kuramoto. *Chemical oscillations, waves and turbulence*, volume 19 of *Springer Series in Synergetics*. Springer-Verlag, Berlin, 1984.
- [14] Jerome V. Moloney and Alan C. Newell. Nonlinear optics. *Phys. D*, 44(1-2):1–37, 1990.
- [15] Shahir Mowlai, Ahmed Roman, and Michel Pleimling. Spirals and coarsening patterns in the competition of many species: a complex Ginzburg–Landau approach. *J. Phys. A*, 47(16):165001, 2014.
- [16] N. Kopell and L.N. Howard. Target pattern and spiral solutions to reaction-diffusion equations with more than one space dimension. *Adv. Appl. Math.*, 2:417–449, 1981.
- [17] John C. Neu. Vortices in complex scalar fields. *Phys. D*, 43(2-3):385–406, 1990.
- [18] Joseph Paultet, Bard Ermentrout, and William Troy. The existence of spiral waves in an oscillatory reaction-diffusion system. *SIAM J. Appl. Math.*, 54(5):1386–1401, 1994.

- [19] L. M. Pismen. Weakly radiative spiral waves. *Phys. D*, 184(1-4):141–152, 2003. Complexity and nonlinearity in physical systems (Tucson, AZ, 2001).
- [20] L. M. Pismen and A. A. Nepomnyashchy. On interaction of spiral waves. *Phys. D*, 54:183–193, 1992.
- [21] R. W. Walden, Paul Kolodner, A. Passner, and C. M. Surko. Traveling waves and chaos in convection in binary fluid mixtures. *Phys. Rev. Lett.*, 55(5):496–499, Jul 1985.
- [22] AN Zaikin and AM Zhabotinsky. Concentration wave propagation in two-dimensional liquid-phase self-oscillating system. *Nature*, 225(5232):535–537, 1970.